© 2017. Published by The Company of Biologists Ltd | Development (2017) 144, 2045-2058 doi:10.1242/dev.139949

RESEARCH ARTICLE

COUP-TFI mitotically regulates production and migration of dentate granule cells and modulates hippocampal Cxcr4 expression

Joséphine Parisot[1,*], Gemma Flore[2,*], Michele Bertacchi[1] and Michèle Studer[1,‡]

ABSTRACT

Development of the dentate gyrus (DG), the primary gateway for hippocampal inputs, spans embryonic and postnatal stages, and involves complex morphogenetic events. We have previously identified the nuclear receptor COUP-TFI as a novel transcriptional regulator in the postnatal organization and function of the hippocampus. Here, we dissect its role in DG morphogenesis by inactivating it in either granule cell progenitors or granule neurons. Loss of COUP-TFI function in progenitors leads to decreased granule cell proliferative activity, precocious differentiation and increased apoptosis, resulting in a severe DG growth defect in adult mice. COUP-TFI-deficient cells express high levels of the chemokine receptor Cxcr4 and migrate abnormally, forming heterotopic clusters of differentiated granule cells along their paths. Conversely, high COUP-TFI expression levels downregulate *Cxcr4* expression, whereas increased *Cxcr4* expression in wild-type hippocampal cells affects cell migration. Finally, loss of COUP-TFI in postmitotic cells leads to only minor and transient abnormalities, and to normal *Cxcr4* expression. Together, our results indicate that COUP-TFI is required predominantly in DG progenitors for modulating expression of the *Cxcr4* receptor during granule cell neurogenesis and migration.

KEY WORDS: Hippocampus, Dentate gyrus, Mouse, COUP-TFI (NR2F1), Granule cells, Cell migration, Cxcr4

INTRODUCTION

The dentate gyrus (DG) is part of the hippocampal formation and the primary input site for excitatory projections to the hippocampus. Its development is more protracted than that of other cortical regions and involves the generation of a progenitor pool that remains active well beyond birth (Altman and Bayer, 1990a,c; Eckenhoff and Rakic, 1988; Li and Pleasure, 2005; Nowakowski and Rakic, 1981; Pleasure et al., 2000; Rakic and Nowakowski, 1981). The major cell type in the DG is the granule cell (GC), the progenitors of which originate from a restricted area of the medial pallium neuroepithelium, the DG neuroepithelium (DGN) or primary (1ry) matrix at around E13.5 in mice. DG progenitors travel along the secondary (2ry) matrix towards the pial side of the cortex and form the dentate migratory stream (DMS), which is composed of a mix of intermediate progenitor cells (IPCs) and postmitotic immature granule neurons. At the end of their migration, GCs accumulate in the DG anlage or hilus and establish a new germinative pool, called the tertiary (3ry) matrix. At this stage, the glial scaffold extends to the hippocampal fissure and pial surface, and directs the migration of dentate precursors (Urban and Guillemot, 2014). Although DG morphogenesis starts early in embryonic development, the vast majority of GCs are generated within the first two postnatal weeks and originate from the 3ry matrix (Muramatsu et al., 2007). Granule cells laminate in an outside-in gradient by which the oldest cells are positioned more superficially and the youngest more deeply, whereas neural stem cells become restricted to the subgranular zone (SGZ), which constitutes one of the two adult neurogenic niches of the mammalian brain (Altman and Bayer, 1990a,b; Altman and Das, 1965; Cowan et al., 1980).

One of the particularities of DG development is that neurogenesis and migration are not independent processes, even if controlled by transcriptional regulators and signalling pathways similar to those described for the neocortex (Hevner, 2016). Lef1, which is a mediator of Wnt signalling, controls the generation of GCs (Galceran et al., 2000), whereas Ngn2 maintains progenitors in an undifferentiated state, allowing them to amplify prior to differentiation into GCs, which is regulated by NeuroD1 (Galichet et al., 2008; Roybon et al., 2009). The IPC factor Tbr2 is required for overall GC neurogenesis and proper migration of Cajal-Retzius cells to the DG (Hodge et al., 2013, 2012). Although most of these factors are widely expressed in several regions of the cortex (Englund et al., 2005), Prox1 is specifically restricted to dentate GCs from early stages to adulthood. Prox1 controls GC amplification, differentiation and maturation (Galeeva et al., 2007; Lavado et al., 2010; Lavado and Oliver, 2007), and postmitotically defines GC identity over the hippocampal pyramidal-like phenotype (Iwano et al., 2012). Migration of GCs requires reelin signalling, expressed by Cajal-Retzius cells, and the Cxcl12/Cxcr4 pathway, which represents the major chemotactic system involved in DG morphogenesis. The ligand Cxcl12 (SDF1) is secreted by meningeal and Cajal-Retzius cells, whereas migrating GCs express the receptor Cxcr4 during prenatal stages (Berger et al., 2007). As a consequence, *Cxcr4* mutant mice exhibit severe DG morphogenesis abnormalities, due mainly to defective GC neurogenesis, migration and final positioning (Bagri et al., 2002; Lu et al., 2002). However, despite these studies, relatively little is known about how factors and signalling molecules interact with each other in controlling GC differentiation and migration.

We have recently demonstrated that the nuclear receptor COUP-TFI (or Nr2f1), which acts as a strong transcriptional regulator (Alfano et al., 2014a), is required for proper hippocampal growth and function (Flore et al., 2017). COUP-TFI mutant mice possess a

[1]Université Côte d'Azur, CNRS, Inserm, iBV, Nice 06100, France. [2]Institute of Genetics and Biophysics, CNR, Naples 80131 Italy.
*These authors contributed equally to this work

‡Author for correspondence (michele.studer@unice.fr)

J.P., 0000-0003-4973-2862; M.S., 0000-0001-7105-2957

Received 30 May 2016; Accepted 24 April 2017

Development (2017) 144, 2045-2058 doi:10.1242/dev.139949

hypomorphic hippocampus, specifically altered in its septal/dorsal pole, and are afflicted by a selective spatial memory deficit (Flore et al., 2017). However, the cellular and molecular causes of this growth defect are not known. To address this issue, we have investigated the role of COUP-TFI during DG morphogenesis from the earliest stages of DG development to adulthood. We first show that COUP-TFI is expressed in the different populations of GC progenitors and postmitotic neurons throughout all stages of DG development. Mitotic disruption of COUP-TFI function leads to the loss of a large fraction of the GC pool and to distinct migratory defects and impaired laminar organisation, resulting in severe DG dysmorphogenesis. *Cxcr4* expression is highly upregulated in the DGN and migrating progenitors of mutant DG. Similarly, forced *Cxcr4* expression in the DG mimics migratory defects in wild-type embryos. Postmitotic COUP-TFI inactivation induces instead only mild and transient defects, with no changes in *Cxcr4* expression. Overall, our study shows that COUP-TFI modulates *Cxcr4* expression levels in GC progenitors, and unravels a novel role for this transcriptional regulator in DG morphogenesis.

RESULTS

COUP-TFI is expressed from the onset of DG development into late postnatal ages

To start addressing COUP-TFI function in DG development, we characterized its distribution in GCs at different stages. At E13.5, COUP-TFI is highly expressed in the DGN located just dorsal to the cortical hem (Fig. 1A) and, by E16.5, in the majority of proliferating and differentiating cells distributed along the three matrices (89% in 1ry, 82% in 2ry and 68% in 3ry matrix; Fig. 1B-C′). Indeed, COUP-TFI is expressed in 81% of proliferating Ki67$^+$ cells, in 96% of Pax6$^+$ radial glia progenitors and in 80% of Tbr2$^+$ IPCs in the 1ry matrix (Fig. 1D-F′), and is highly colocalized with Prox1 in GC precursors and differentiating neurons (Fig. 1G,G′). Between birth and P14, COUP-TFI is maintained in all postmitotic GCs (Fig. 1H-J), as confirmed by a high rate of colocalization with Prox1 in GCs (Fig. 1K-M,Q), with the glutamatergic marker Tbr1 in differentiating GCs (Fig. 1N-Q), and with the neuronal marker NeuN (Rbfox3) at P7 and P14 in mature GCs (Fig. 1Q-S). Thus, COUP-TFI labels all phases of GC neurogenesis in the developing DG from cycling progenitors to postmitotic and mature neurons.

COUP-TFI inactivation in progenitors results in progressive DG growth impairments

To directly investigate COUP-TFI role during DG development from its onset to its final formation, we used the *COUP-TFIf/f*^{EmxCre} conditional line, referred to throughout this study as *EmxCKO* (Fig. 2A,A′), in which COUP-TFI is completely absent in all cells of the developing and postnatal DG and in all Prox1$^+$ GCs (Fig. 2B-D′). Although no particular growth defect was observed at E16.5, the whole *EmxCKO* DG shows a slightly reduced volume at birth (Fig. 2E,E′,I), in which its septal region is 51% smaller than the control (Fig. S1A), in line with the selective hippocampal reduction we have previously described (Flore et al., 2017). By P7, the total volume of the mutant DG is decreased to 68% of its normal size (Fig. 2I′) with both blades reduced in length and thickness, and accumulation of ectopic cells in the hilus (Fig. 2F′). The growth defect remains evident at P14, with a total reduction of 45%, shorter blades (Fig. 2G,G′,I″) and a more pronounced defect in the septal pole compared with the temporal pole (Fig. S1A′,A″). Growth impairments are even more exacerbated in 2-month-old mutants: the DG is only 29% of its normal size (Fig. 2H,H′,J), the upper and lower blades show a 69% and 72% reduction in size, respectively (Fig. 2J′,J″), and the volume of the DG is dramatically affected along the septo-temporal axis (Fig. S1B). However, adult *EmxCKO* DG, in contrast to P7 and P14 *EmxCKO* DG, depict a rather normal layer organisation, with a sharp hilus/granule cell layer (GCL) boundary (Fig. 2H′), suggesting that ectopic hilar cells eventually reach their final position. Overall, these data indicate very little postnatal DG growth in *EmxCKO* mutants (Fig. 2K), and suggest that COUP-TFI plays a major role in promoting growth and expansion of the developing DG, particularly in its septal region.

Early progenitors precociously differentiate into granule cells in *COUP-TFI* loss-of-function mutants

To decipher the cellular mechanisms underlying the mutant morphogenetic defects, we evaluated the capacity of GC progenitors to properly expand at E16.5. The proliferation marker Ki67 indicates a 28% reduction in the number of cycling cells in the ventricular zone (VZ) of the 1ry matrix and a 51% reduction in the number of migrating progenitors in the *EmxCKO* DG septal primordium (Fig. 3A-A″), whereas no differences were found in the 1ry matrix of the temporal DG (Fig. S1C). This was also confirmed by a significant reduction in the number of proliferating cells in S-phase, as observed after a short pulse of EdU in E16.5 embryos (Fig. 3B-B″). To further understand the types of GCs affected in *EmxCKO* mutants, E16.5 DG was stained either with EdU injection and Pax6, to label proliferating progenitors, including most of the radial glia cells (Gotz et al., 1998) (Fig. 3C-C″), or with Tbr2 and the replication marker Mcm2, to label proliferating IPCs (Fig. 3D-D″). The amount of cycling progenitors and IPCs was drastically reduced in mutant mice (decreased by 43% for progenitors; and by 82%, 77% and 86% in the 1ry, 2ry and 3ry matrices, respectively, for IPCs) (Fig. 3C″,D″). By injecting EdU 24 h before sacrifice and labelling EdU$^+$ cells with the proliferation marker Ki67 at E16.5, we calculated the amount of cells that were proliferating at the time of injection (EdU$^+$) but had since exited the cell cycle (Ki67$^-$) (Fig. 3E-E″). This cell-cycle exit index (EdU$^+$Ki67$^-$/EdU$^+$) shows a 34% increase in *EmxCKO* 1ry matrix compared with control, indicating that these cells have precociously exited their cell cycle. Moreover, among the Tbr2$^+$ population, 50% more Tbr2$^+$Prox1$^+$ cells were detected in the future DG (Fig. 3F-F″), supporting precocious differentiation of IPCs into GCs in mutant newborns. Finally, E14.5 embryos, pulse-chased with EdU and labelled with Prox1 at P0, show the same proportion of EdU$^+$Prox1$^+$ cells among all EdU$^+$ cells in control and mutant DG (Fig. 3G-G″), confirming that early progenitors do normally adopt a neurogenic granular fate in *EmxCKO* mutants. Hence, our data indicate that COUP-TFI regulates expansion of both Pax6$^+$ radial glia and Tbr2$^+$ IPC pools in a timely manner during DG development (Fig. 3H).

Prolonged defects in cell proliferation and differentiation lead to a smaller DG in postnatal *EmxCKO* mutants

Next, we evaluated whether abnormalities in the IPC pool are protracted during postnatal stages in mutant mice (Fig. 4). A decreased number of proliferating IPCs (Mcm2$^+$Tbr2$^+$ cells) are maintained in the 3ry matrix of *EmxCKO* DG at P0 (Fig. 4A-B″), indicating that even during the growth phase, DG cells maintain reduced proliferative capacities. Accordingly, 12% more Prox1$^+$ GCs were observed in P7 *EmxCKO* DG (Fig. 4C,C′,F) and most probably become NeuN$^+$ neurons (Fig. 4D,D′,F′). The proportion of NeuN$^+$ neurons in the GCL is not affected in P14 *EmxCKO* DG, despite its reduced size (Fig. 4E,E′,F″),

Development (2017) 144, 2045-2058 doi:10.1242/dev.139949

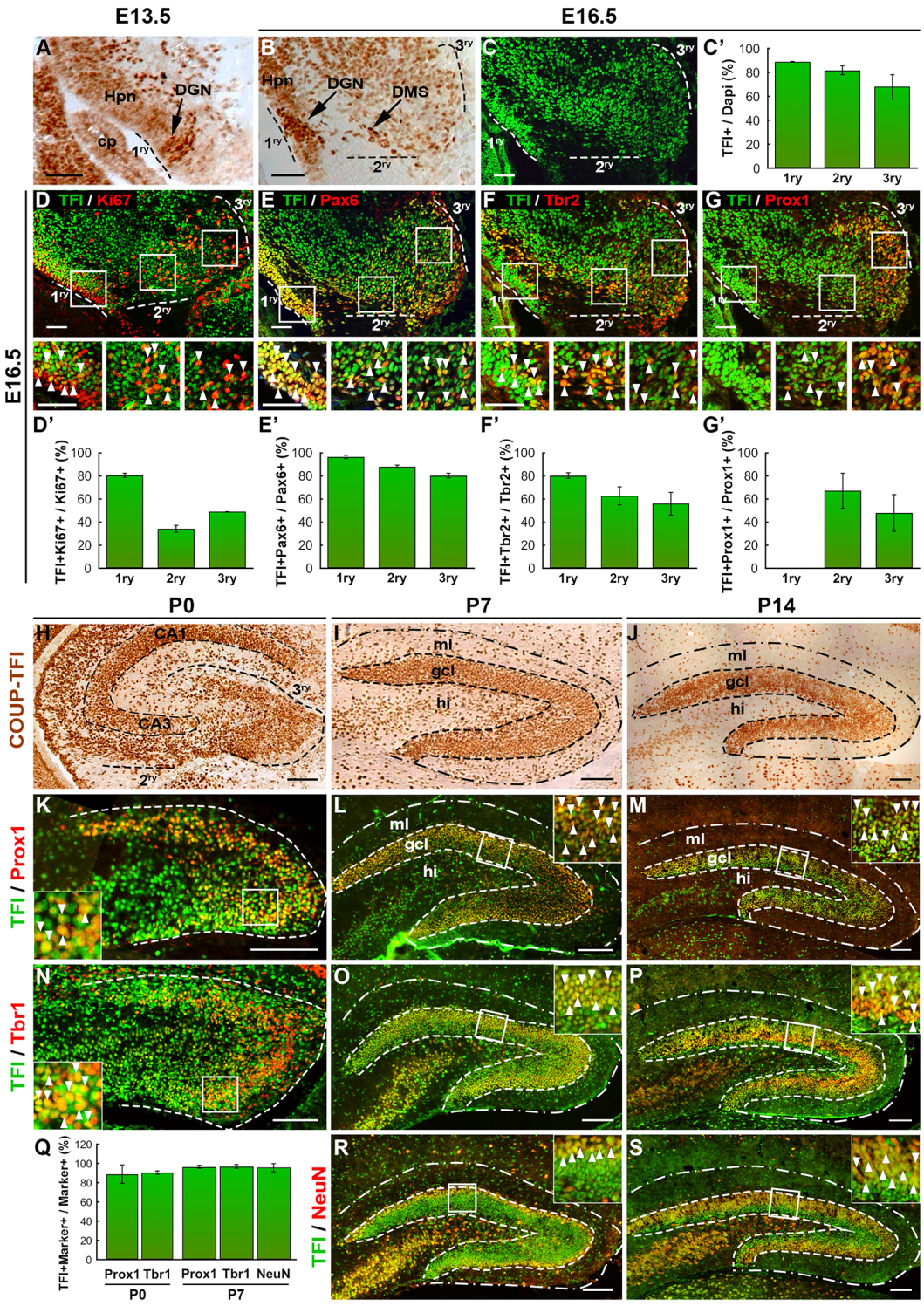

Fig. 1. COUP-TFI is expressed in the developing dentate gyrus from its onset to late postnatal stages. (A-C′) Details of coronal sections of E13.5 (A) and E16.5 (B,C) embryos showing COUP-TFI localisation by immunohistochemistry (A,B) and immunofluoresence (C). The amount of COUP-TFI^{+} cells in each matrix is represented in C′. (D-G) Immunofluoresence showing the colocalization of COUP-TFI with Ki67, Pax6, Tbr2 and Prox1. (D′-G′) Quantification of the percentage of marker-positive cells expressing COUP-TFI. (H-J) Immunohistochemistry of COUP-TFI in the postnatal DG. (K-S) Co-expression of COUP-TFI with Prox1, Tbr1 and NeuN at indicated ages. (Q) Quantification of the percentage of marker-positive cells expressing COUP-TFI in the DG. Arrowheads in the high-magnification views and insets indicate double-labelled cells. cp, choroid plexus; DGN, DG neuroepithelium; DMS, dentate migratory stream; gcl, GC layer; hi, hilus; Hpn, hippocampal neuroepithelium; ml, molecular layer. Scale bars: 50 µm in A-G; 100 µm in H-S.

and granule neurons acquire a mature morphology, as highlighted by the reporter line *Thy1-eYFP-H* (Fig. 4G-H′). This suggests that COUP-TFI acts preferentially during the early prenatal phases of granule cell proliferation and differentiation rather than during the late postnatal phase of cell differentiation and maturation.

Development (2017) 144, 2045-2058 doi:10.1242/dev.139949

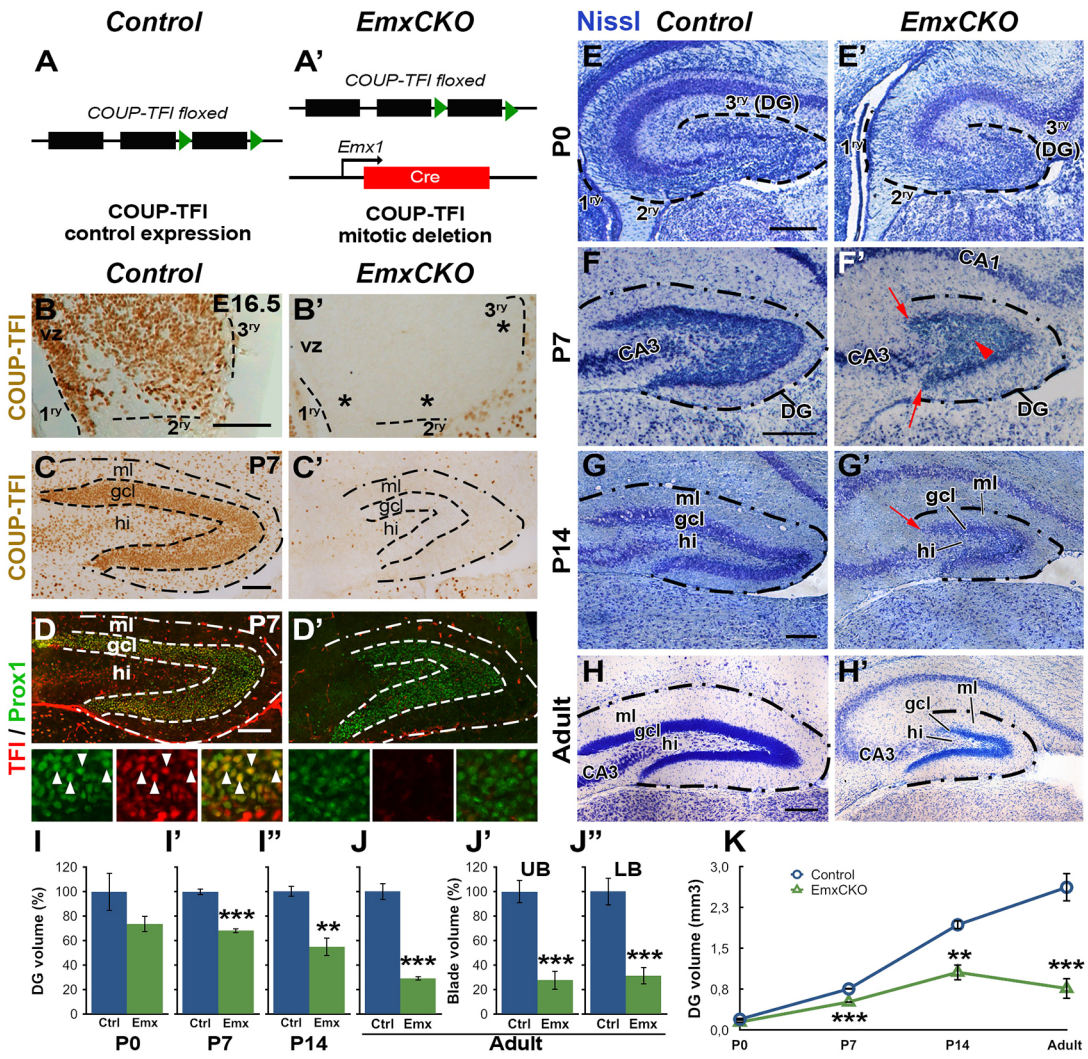

Fig. 2. COUP-TFI mitotic inactivation results in severe DG growth defects. (A,A′) Genetic strategy for mitotic COUP-TFI inactivation. (B-D′) Validation of COUP-TFI loss of function by immunohistochemistry or immunofluoresence on coronal sections. Asterisks in B′ indicate absence of COUP-TFI protein from the three matrices at E16.5. No COUP-TFI protein is expressed in GCs and Prox1$^+$ cells in *EmxCKO* at P7 (C′,D′). (E-H′) Nissl staining of control and *EmxCKO* DG at the ages indicated. The red arrowhead in F′ indicates the hilus filled with cells, arrows in F′ and G′ show shortening of the blade length in *EmxCKO*. (I-I″) Relative total DG volume at the ages indicated. (J-J″) Total DG volume and upper (UB) and lower (LB) blade volumes in adult controls and *EmxCKO*. (K) Total DG volume in mm^3 from P0 to adult stages, illustrating a gradual growth deficiency in *EmxCKO* DG. gcl, GC layer; hi, hilus; ml, molecular layer; vz, ventricular zone. Scale bars: 100 µm in B-D′; 200 µm in E-H′. $^{**}P\leq0.01$; $^{***}P\leq0.001$.

Aberrant GC migration and laminar organisation in the *EmxCKO* postnatal dentate gyrus

We hypothesized that, besides impairments in cell proliferation, the reduced postnatal growth observed in mutant DG might also be due to abnormal migration. Tbr2$^+$ cells normally engage two distinct migratory paths at birth: one around the DG pole of the 3ry matrix to form the transient subpial neurogenic zone (SPZ) and one towards the hilus (Fig. 5A) (Hodge et al., 2013). In both regions, cells undergo further rounds of expansion and form the second germinative zone. In *EmxCKO* mutants, Tbr2$^+$ IPCs abnormally migrate along the DMS: cells are more spread out compared with the narrow stream in controls, and more Tbr2+ ectopic cells are found migrating towards the prospective SPZ of the hilus (Fig. 5A,A′). By P7, numerous Tbr2$^+$ cells are grouped at the lower blade tip in controls (Fig. 5B), but not in mutant DG, where ectopic cells are found either along the 2ry matrix or in the lower blade molecular layer (Fig. 5B′). At P14, Tbr2$^+$ cells are aligned along the future adult SGZ niche (Fig. 5C), whereas mutant cells are abnormally dispersed within the GC and molecular layers (Fig. 5C′), as also confirmed by the altered radial distribution of Mcm2$^+$ and Tbr2$^+$ cells (Fig. 5D,D′). Ectopically located cells fail to properly laminate the GCL, as substantial amounts of Prox1$^+$ cells are widely dispersed in the hilus or differentiate *in loco*, as confirmed by the presence of ectopic cellular aggregates in the molecular layer and/or in the area that resembles the DMS (Fig. 5E-F′). These clusters mature into Tbr1$^+$ and NeuN$^+$ granule neurons and are still evident at P14 (Fig. 5G′,H′). On the contrary, no GC lamination defects can be found in the temporal pole of *EmxCKO* DG, confirming a preferential alteration in septal DG (Fig. S1D,D′). Thus, COUP-TFI seems to control the migration of GCs along the DMS and within the septal DG.

Aberrant glial scaffolding prevents proper GC positioning of the postnatal SGZ

To further decipher the mechanisms underlying the abnormal DG laminar organisation in mutants, we stained E13.5 to adult DG with

Development (2017) 144, 2045-2058 doi:10.1242/dev.139949

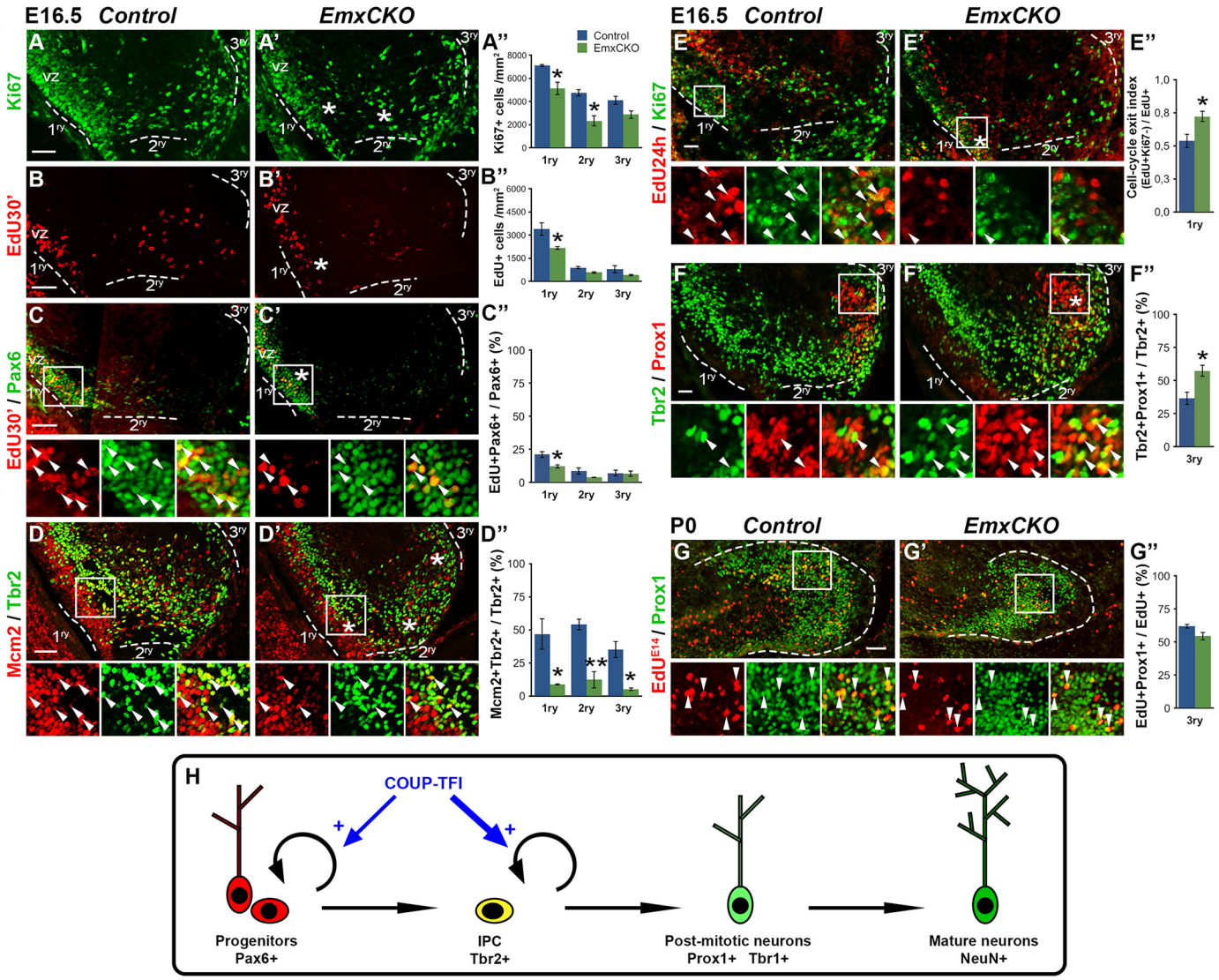

Fig. 3. COUP-TFI loss affects the proliferative and differentiating capacities of progenitors and IPCs at prenatal stages. (A-F′) Coronal sections of control and *EmxCKO* E16.5 septal DG immunostained with the markers indicated on the left. (B-C′) Control and mutant embryos were pulse-labelled with EdU for 30 min. Below each panel are high-magnification views of single- and double-positive cells (arrowheads). (A″-F″) Associated cell counts representing the density of labelled cells in the indicated matrices. E″ is the cell-cycle exit index and corresponds to the (EdU$^+$Ki67$^-$)/EdU$^+$ ratio. (G-G″) Cell fate of early born GCs in control and *EmxCKO* DG. Arrowheads indicate double-labelled cells in high-magnification views. G″ represents the percentage of E14.5 born cells (EdU$^+$) that had differentiated into Prox1$^+$ GCs by P0. (H) Proposed model for COUP-TFI function in early GC neurogenesis: COUP-TFI promotes expansion of the progenitors and IPC pool (+) in a timely manner. The differences in thickness of the blue arrows indicate a stronger effect on IPCs versus apical progenitors. Asterisks in IF panels indicate presence of significant changes in cell numbers as confirmed by corresponding cell counts. VZ, ventricular zone. Scale bars: 50 µm. *P≤0.05; **P≤0.01.

brain lipid-binding protein (BLBP) and/or glial fibrillary acidic protein (GFAP) to follow radial glia cells that form the primary scaffold along the hilus and the secondary scaffold across the GCL. During embryonic stages, no obvious fibre morphology or orientation defects were detected in *EmxCKO*s (Fig. S2), similar to the neocortex (Alfano et al., 2011). At birth, GFAP$^+$ fibres project radially across the hilus and progenitors migrate along their processes before reaching the SPZ (Fig. 6A,B). By contrast, GFAP$^+$ fibres are abnormally oriented in mutant DG, and migrating Tbr2$^+$ cells acquire a disorganized pattern within the forming dentate (Fig. 6A′-B′) that could partially explain the aberrant routes undertaken by Tbr2$^+$ cells at this stage (Fig. 5A′). Next, we investigated the morphology of the secondary (or transgranular) radial glia scaffolding, which is required at postnatal stages for the GC subpial to granular transition (Brunne et al., 2010). By P7, radial glia fibres have reached the molecular layer, and their cell bodies (visualized by BLBP) accumulate along the inner GCL (Fig. 6C,D). This late scaffold is fully established at P14, and SGZ cells are now aligned at the lowermost border of the GCL (Fig. 6E). Radial glia cells appear poorly organized in P7 and P14 *EmxCKO* DG: their BLBP$^+$ somata are abnormally spread within the GCL, and GFAP$^+$ shorter processes lack the characteristic orientation (Fig. 6C′-E′). This abnormal morphology is maintained throughout adulthood, in which star-like mutant GFAP$^+$ cells strikingly differ from the elongated radial processes observed in control DG (Fig. 6F-G′). Finally, we evaluated the capacity of adult stem cells to proliferate and observed a decrease of more than 50% of BrDU$^+$ cells in *EmxCKO* DG (Fig. 6H-J). Taken together, loss of COUP-TFI in early DG progenitors affects the formation of a proper radial glia scaffold, which ultimately impinges on the migration, morphology

Development (2017) 144, 2045-2058 doi:10.1242/dev.139949

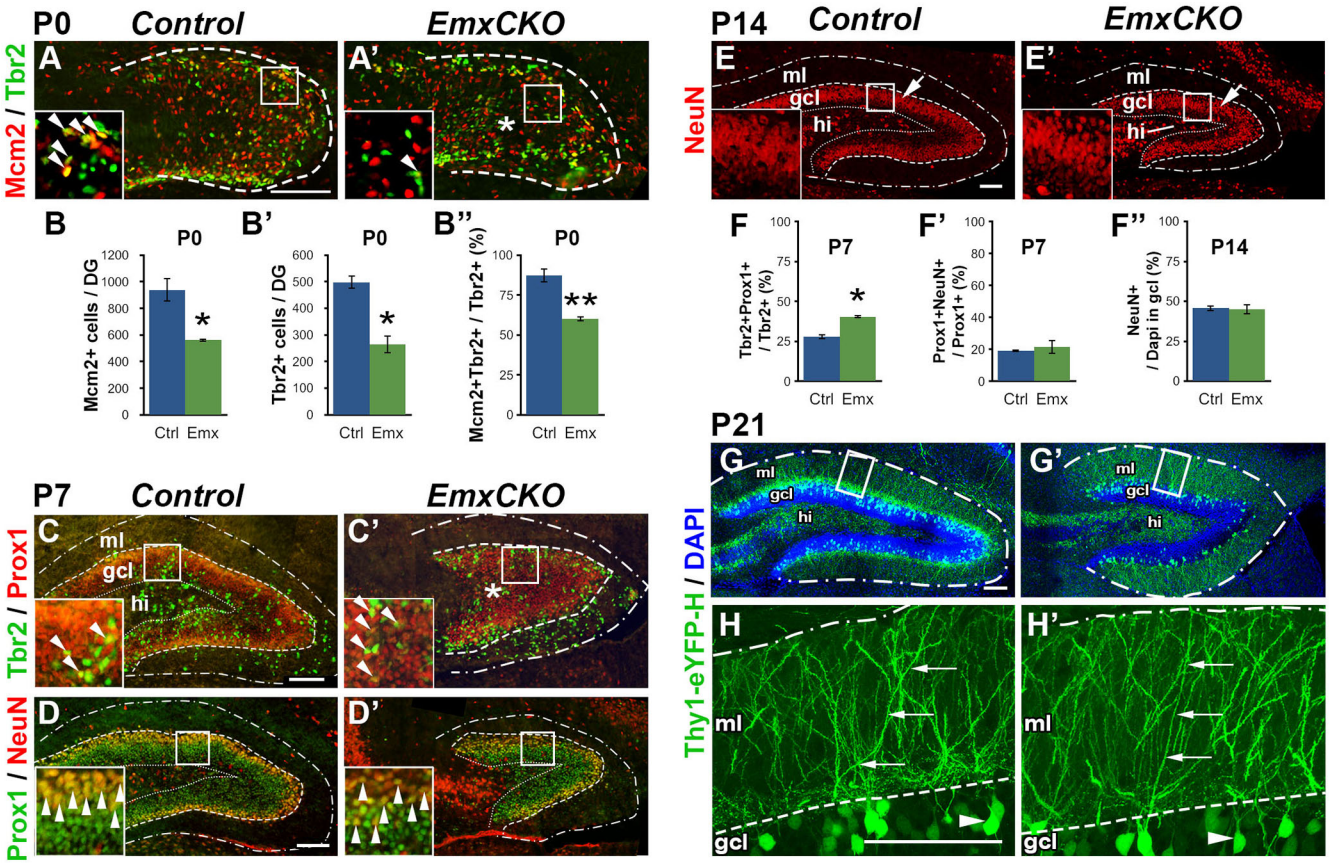

Fig. 4. Reduced number of cells but proper GC maturation in postnatal *EmxCKO* mutants. (A,A′) Coronal sections of septal DG of P0 control and *EmxCKO* stained with Mcm2 and Tbr2 labelling proliferating IPCs. Arrowheads in insets indicate double-positive cells. Asterisk in A′ illustrates the reduction in mitotic cells. (B-B″) Quantification of marker-positive cells at P0. (C-D′) Coronal sections of septal DG of P7 control and *EmxCKO* stained with Tbr2/Prox1 and Prox1/NeuN, labelling early differentiating IPCs and late differentiating GCs, respectively. Arrowheads in insets indicate double-positive cells. (E,E′) NeuN expression restricted to the uppermost GC layer (arrows) in control and *EmxCKO* DG at P14. (F-F″) Quantification of differentiating IPCs (F), Prox1$^+$ GCs (F′) and differentiated NeuN$^+$ GCs (F″) at P7 and P14. (G-H′) YFP staining of somata and dendrites of P21 control and *EmxCKO* DG labelling mature GCs. (H,H′) *Z*-stack maximum intensity projections of the boxes in G,G′. Arrows indicate a dendrite and arrowheads indicate a GC soma. gcl, GC layer; hi, hilus; ml, molecular layer. Scale bars: 100 µm. *$P\leq0.05$; **$P\leq0.01$.

and, possibly as a secondary consequence, final establishment of the adult neurogenic niche.

Postmitotic inactivation of COUP-TFI does not alter DG growth or granule cell differentiation

As COUP-TFI is expressed in both mitotic and postmitotic cells during DG development, we wondered whether absence of solely postmitotic COUP-TFI function would recapitulate part of the *EmxCKO* phenotype. To investigate this, the *COUP-TFI$^{flox/flox}$* mouse line was crossed to the *Nex-Cre* mouse, which acts in early differentiating cortical neurons (Alfano et al., 2014b; Goebbels et al., 2006) (Fig. 7A,A′). In the resulting progeny (herein referred to as *NexCKO*), COUP-TFI is maintained in the VZ of the 1ry matrix and in migrating Tbr2$^+$ IPCs from E16.5 to P7, but depleted in pyramidal hippocampal neurons and in the majority of Prox1$^+$ and Tbr1$^+$ GCs (Fig. 7B-C′; Fig. S3), while being maintained in Gad67$^+$ interneurons (Fig. S3D,D′). Thus, in contrast to the *EmxCKO* mouse mutant, COUP-TFI protein is maintained in cycling progenitors in the *NexCKO* mouse model, allowing us to assess its unique function in postmitotic neurons during DG morphogenesis.

Notably, mutant *NexCKO* DG show no significant size reductions from P0 to P14 (Fig. 7D-G; Fig. S4A-A″), even if they tend to have a slightly smaller volume than control littermates (Fig. 7G) and depict a rounded C-shape instead of the characteristic V-shape of littermate controls (Fig. 7E-F′; Fig. S4B,B′). In 2-month-old *NexCKO* brains, the DG volume is again slightly, but not significantly, reduced compared with control (Fig. S4C), and no statistically significant differences in the entire hippocampal volume and its septo-temporal distribution are found (Fig. S4D-D″). Overall, this indicates that COUP-TFI plays no major postmitotic role in global hippocampal morphogenesis.

Characterization of the proliferation and differentiation potentials of GC progenitors in E16.5 and P0 *NexCKO* DG revealed no defects in the number and distribution of cycling and differentiating Tbr2$^+$ IPCs (Fig. S4E-I′). However, we found a slight disorganization of GFAP$^+$ fibres in the primary radial scaffold at P0 (Fig. 7H-I′), even if not as severe as in *EmxCKO* (Fig. 6A-B′), and several Prox1$^+$ cells are abnormally distributed in the forming hilus (Fig. 7J′). Similarly, glia fibres of the transgranular scaffold are slightly affected in the *NexCKO* mutants at P7, and BLBP$^+$ somata are more disorganized in the GCL of mutants compared with controls (Fig. 7K,K′). However, these defects are rescued by P14, by which time BLBP$^+$, as well as Mcm2$^+$ and Tbr2$^+$, cells are now properly aligned in the inner region of the GCL (Fig. 7L-N′). Moreover, both the position and number of NeuN$^+$ mature GCs are similar to those in controls in *NexCKO* DG (Fig. S4J,J′), indicating that the minor abnormalities observed in the *NexCKO* pups are fully rescued by late developmental stages. Thus, the absence of postmitotic

Development (2017) 144, 2045-2058 doi:10.1242/dev.139949

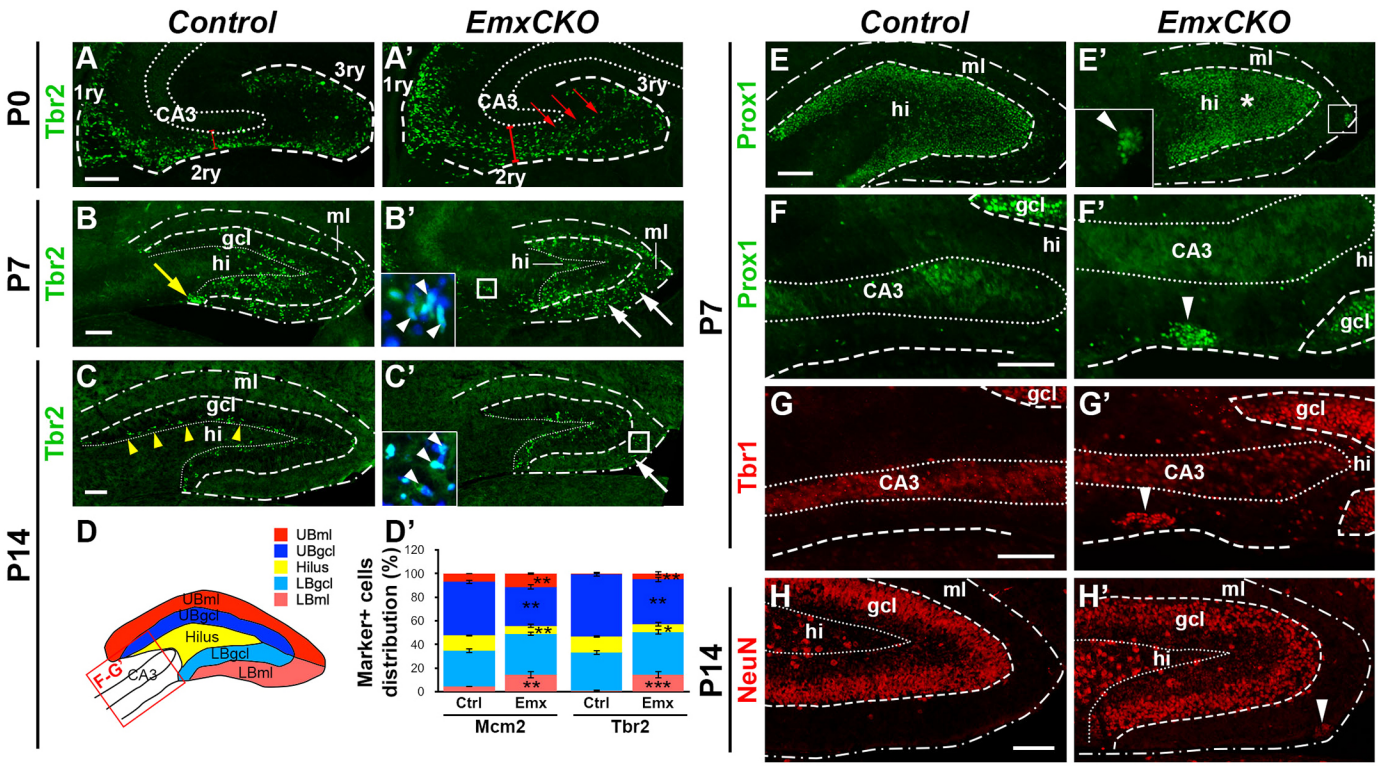

Fig. 5. COUP-TFI inactivation induces aberrant GC migration and laminar organization in postnatal DG. (A,A′) Tbr2$^+$ cells in coronal sections of P0 control and *EmxCKO* DG. Red bars delineate the stream of migrating cells and red arrows indicate ectopic cells in the 3ry matrix. (B,B′) Yellow arrow indicates Tbr2$^+$ cells at the lower tip of the P7 control DG. (C,C′) Yellow arrowheads indicate aligned mitotic cells in the future P14 SGZ in controls. In B′ and C′, white arrows indicate numerous cells in the molecular layer (ml) of mutants and arrowheads in the insets indicate ectopic cells (Tbr2$^+$DAPI$^+$) in the 2ry matrix. (D,D′) Quantification of the distribution of Mcm2$^+$ and Tbr2$^+$ cells along five distinct layers. (E,E′) The asterisk indicates ectopic presence of Prox1$^+$ cells populating the hilus of *EmxCKO* DG at P7. Inset in E′ shows a representative ectopic Prox1$^+$ cell aggregate in the molecular layer. (F-G′) High-magnification views of the red box in D showing heterotopic clusters (arrowheads) of Prox1$^+$ and Tbr1$^+$ cells in the *EmxCKO* at P7. (H,H′) Presence of clusters (arrowhead) of mature NeuN$^+$ cells in P14 *EmxCKO* lower blade molecular layer. All layers are delimited based on DAPI staining. gcl, GC layer; hi, hilus; ml, molecular layer; UB/LB, upper/lower blade. Scale bars: 100 µm. *P≤0.05; **P≤0.01; ***P≤0.001.

COUP-TFI has a minor effect on the organisation of the glia scaffold that does not seem to affect differentiation and migration of granule cells, and ultimately DG growth.

Finally, to assess whether cell death could partially contribute to the morphological defects observed in *EmxCKO* and *NexCKO* mutants, we labelled E16.5 and P0 DG with active-caspase 3 (Fig. S5), which marks cells undergoing apoptosis (Porter and Janicke, 1999). Even if no cell death can be detected in COUP-TFI mutants at E16.5 (Fig. S5A-A″,B), a significant amount of dying cells are found at P0 in septal, but not temporal, regions of *EmxCKO* and *NexCKO* mutant DG (Fig. S5C-D′). A concentration of dying cells is surprisingly localized in the subiculum of *NexCKO* brains (Fig. S5C″), most probably leading to the scattered subiculum cell layer and contributing to the abnormal rounded shape of *NexCKO*-affected DG (Fig. S5E″). Thus, this differential apoptotic pattern might partially contribute to the distinct morphological defects observed in the two strains of mutant mice.

COUP-TFI modulates Cxcr4 expression levels in progenitors during hippocampal cell migration

In light of the similar DG defects observed in both *Cxcr4* and *EmxCKO* mutant mice, we hypothesized that COUP-TFI-deficient GCs might abnormally respond to chemokine Cxcr4/Cxcl12 signalling (Bagri et al., 2002; Berger et al., 2007; Li et al., 2009; Lu et al., 2002). *Cxcr4* is mainly localized in migrating progenitors and immature GCs (Fig. 8A-D), whereas its ligand *Cxcl12* is normally expressed by meningeal and Cajal-Retzius cells around the dentate pole and in the hippocampal fissure (Fig. S6A-C). Notably, we found a drastic upregulation of the *Cxcr4* transcript in the 1ry matrix, in migrating precursors along the DMS and in the forming DG of E16.5 *EmxCKO* embryos (Fig. 8A′). High transcript and protein levels are maintained in cells of P0 *EmxCKO* hippocampi, as also confirmed by quantitative reverse-transcriptase PCR (qRT-PCR) (Fig. 8B-C′,E,E′). Expression levels are similar to controls at P7 (Fig. 8D,D′), indicating that upregulation of *Cxcr4* is mainly restricted to prenatal stages. Moreover, no changes in *Cxcl12* transcript levels are observed from E16.5 to P7 *EmxCKO* (Fig. S6A-C′) and expression of both *Cxcr4* and *Cxcl12* is not altered in E16.5 *NexCKO* DG (Fig. 8F,F′; Fig. S6D,D′). To further support the role of COUP-TFI in regulating *Cxcr4* expression in progenitors, we used a complementary approach by crossing the *Cre*-dependent *hCOUP-TFI-floxed* transgenic line (Alfano et al., 2014b) with *Emx1-Cre*, thus allowing overexpression of COUP-TFI in all hippocampal progenitors (Fig. 8G-H′). As expected from the loss-of-function data, high COUP-TFI levels downregulate Cxcr4 in the hippocampus (Fig. 8I,I′), confirming that COUP-TFI can modulate *Cxcr4* expression in progenitor cells.

COUP-TFI has also been shown to regulate *Cxcr4* expression in breast cancer cells (Boudot et al., 2014), suggesting that Cxcr4 might be a direct target of COUP-TFI during cell migration. To investigate this, we examined whether COUP-TFI protein could directly bind to the regulatory regions of the *Cxcr4* locus. With the

Development (2017) 144, 2045-2058 doi:10.1242/dev.139949

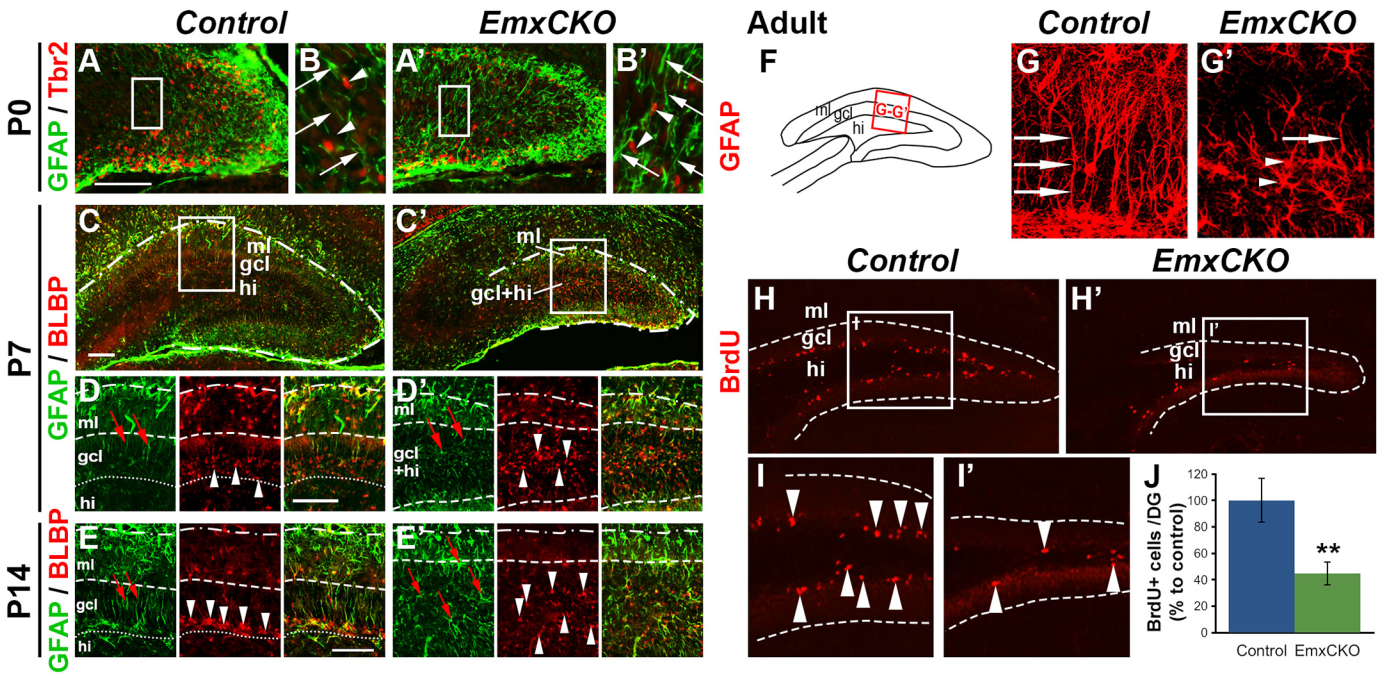

Fig. 6. Aberrant primary and secondary glia scaffolds in postnatal COUP-TFI-deficient dentate gyri and impaired proliferation of the adult neurogenic niche. (A-B′) Coronal sections of P0 control and *EmxCKO* mutants showing the GFAP$^+$ glia scaffold organisation in the 3ry matrix. Arrows in B,B′ indicate GFAP$^+$ fibres and arrowheads indicate migrating Tbr2$^+$ cells along the fibres. (C-E′) Coronal sections of P7 and P14 control and *EmxCKO* DG stained for GFAP labelling fibres (red arrows) and BLBP labelling cell bodies (white arrowheads) of radial glia cells. (D-E′) High magnification views of the DG upper blade. (F-G′) Confocal images of a detail in the adult GC layer (illustrated in F) depict GFAP$^+$ cells with trans-granular fibres (arrows) in controls and mainly star-like cells (arrowheads) in *EmxCKO* adults. (H,H′) Coronal sections of control and *EmxCKO* adult DG labelled for proliferating (BrdU$^+$) cells (arrowheads). (I,I′) High magnifications of the boxes in H,H′. (J) Quantification of BrdU$^+$ cells in control and mutant DG. gcl, GC layer; hi, hilus; ml, molecular layer. Scale bars: 100 µm. $^{**}P \leq 0.01$.

help of the ECR browser (Loots and Ovcharenko, 2007; Quandt et al., 1995), we found a highly conserved COUP-TFI-binding site in the 3′UTR region of the *Cxcr4* locus (Fig. 8J). Chromatin immunoprecipitation (ChIP) on P0 hippocampal cells shows specific binding of COUP-TFI on the fragment amplified from the 3′UTR of *Cxcr4* (Fig. 8J′). Thus, COUP-TFI modulates *Cxcr4* expression levels by binding to its DNA sequence, most probably in a direct manner, although we cannot exclude that co-factors may also participate to this regulation (Fig. 8K).

Finally, as loss of Cxcr4 function seems to affect GC migration (Lu et al., 2002), we overexpressed Cxcr4 in wild-type hippocampal cells by *in utero* electroporation to evaluate whether high Cxcr4 levels would also affect their migration, as observed in *EmxCKO* mutants. First, we confirmed that our *pCIG2-Cxcr4-IRES-GFP* construct is indeed producing high levels of Cxcr4 protein in regions in which Cxcr4 is normally expressed at low levels (Fig. S7). Then, we quantified the distribution of electroporated GFP$^+$ cells in CA1 and DG regions, and showed that cells containing high Cxcr4 depict a significant delayed migration in both areas, when compared with cells electroporated with a control *pCIG2-IRES-GFP* plasmid (Fig. 9). Indeed, a higher proportion of GFP$^+$ cells is detected in the VZ of the CA1 and in the 1ry DG matrix, whereas a lower proportion of GFP$^+$ cells is instead observed in the CA1 pyramidal cell layer and 3ry DG matrix, respectively (Fig. 9B′,D′). Hence, abnormally high levels of Cxcr4 alter hippocampal cell migration in a cell-autonomous way.

DISCUSSION

The DG is one of the few brain areas where progenitors proliferate and generate neurons throughout life. Understanding the molecular and cellular mechanisms governing its morphological development is thus crucial for a full comprehension of its function, including its capacity to generate new neurons throughout adulthood. In this study, we unravel for the first time a key function of the transcriptional regulator COUP-TFI in DG development. We have previously shown that COUP-TFI is required for proper growth and morphogenesis of the hippocampal septal pole and its connectivity to the entorhinal cortex (Flore et al., 2017), but the origin and mechanisms of these defects have not been elucidated. Here, we show that COUP-TFI is highly expressed in the dentate primordium and maintained in all precursors during migration and differentiation, thus representing one of the few transcription factors expressed throughout all stages of DG morphogenesis. Then, we directly assessed its function in DG progenitors or postmitotic granule cells and showed that COUP-TFI is required mainly in GC expansion and migration in the septal DG pole, but not in GC specification and maturation. Using loss- and gain-of-function approaches, we showed that COUP-TFI modulates *Cxcr4* expression leading to abnormal migration of hippocampal precursors (summarized in Fig. 10), and that increased levels of Cxcr4 affect cell migration. Overall, our study contributes to the further dissection of the molecular signature required in the formation and morphogenesis of the DG.

A novel factor required in DG development

It is well established that distinct developmental steps are required in DG morphogenesis during pre- and early postnatal development: proper patterning of the DGN by the nearby cortical hem, correct amplification of progenitors, organisation of the glia scaffolding and transformation of the tertiary matrix before full differentiation of DG neurons (reviewed by Li and Pleasure, 2005). All these

Development (2017) 144, 2045-2058 doi:10.1242/dev.139949

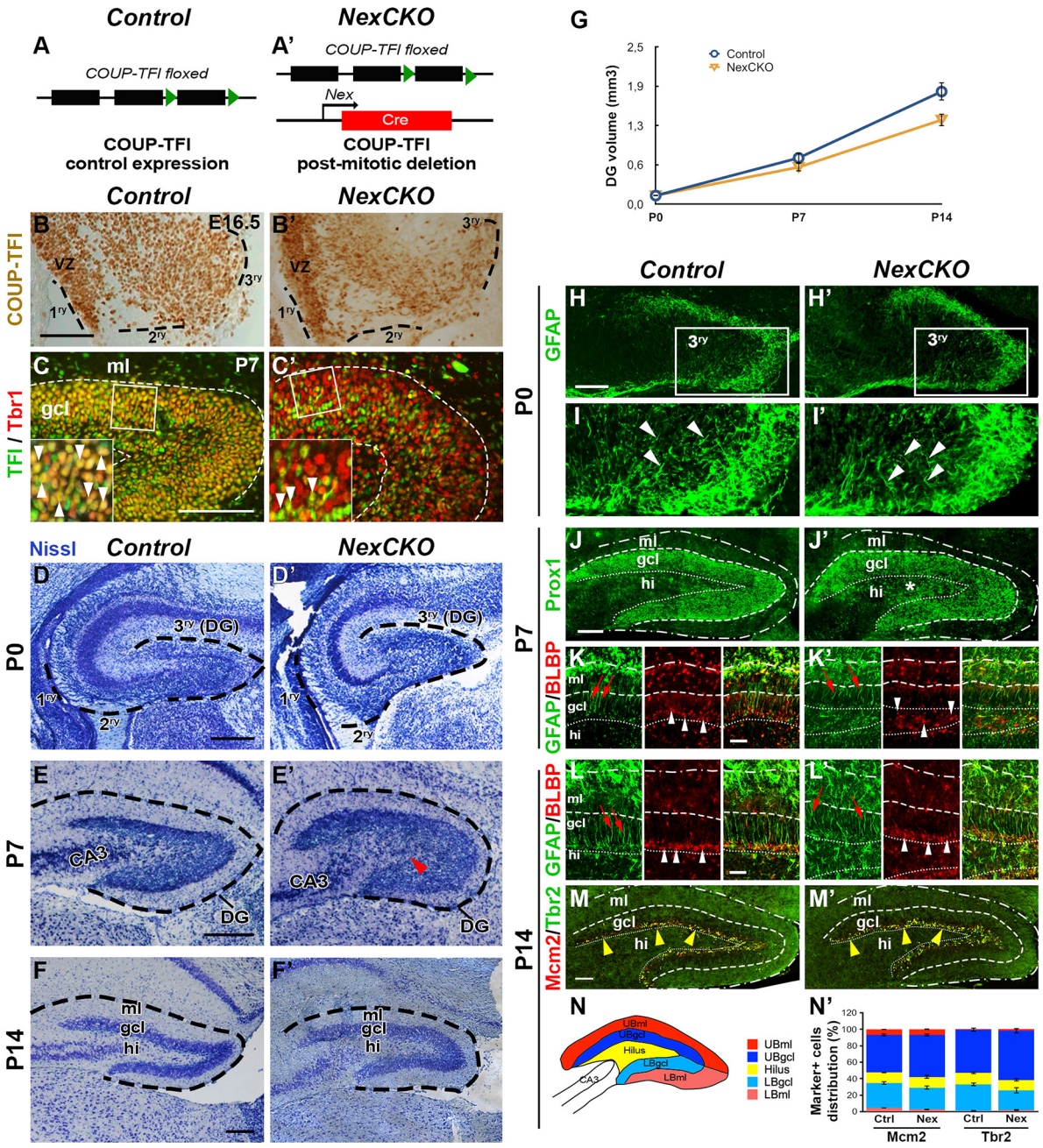

Fig. 7. Postmitotic deletion of COUP-TFI induces mild defects. (A,A′) Genetic strategy for postmitotic conditional COUP-TFI inactivation. (B-C′) COUP-TFI protein is still expressed by mitotic cells at E16.5 (B,B′), but is depleted from Tbr1$^+$ cells in the GC layer at P7 (C,C′). Arrowheads in insets indicate double-labelled cells. (D-F′) Nissl staining of control and *NexCKO* coronal sections of P0, P7 and P14 DG. Red arrowhead in E′ indicates the mutant hilus filled with cells, but this defect is rescued by P14 (F′). (G) Total DG volume in mm^3 during postnatal development. (H-I′) GFAP labelling of the primary glia scaffold at P0; arrowheads indicate fibres. (J,J′) Asterisk indicates ectopic Prox1$^+$ cells in the hilus of *NexCKO* mutants. (K-L′) GFAP$^+$ fibres (red arrows) and BLBP$^+$ cell bodies (arrowheads) of the secondary radial glia scaffold at P7 and P14. (M-N′) Distribution (arrowheads) and quantification (N,N′) of Mcm2$^+$ and Tbr2$^+$ cells at P14. gcl, GC layer; hi, hilus; ml, molecular layer; UB/LB, upper/lower blade; vz, ventricular zone. Scale bars: 100 µm in B-C′,J,J′,M,M′; 200 µm in D-F′; 50 µm in K-L′.

events are controlled by the sequential expression of several transcription factors and signalling pathways (reviewed by Sugiyama et al., 2013; Urban and Guillemot, 2014). Our study reveals that COUP-TFI plays multiple roles during DG development. On the one hand, it is required for overall growth of the septal DG by specifically regulating the progenitor pool during pre- and perinatal stages of development. The reduced progenitor population will then impact on the establishment of the secondary germinative zone in the DG, thus compromising its ultimate expansion and growth. However, even if in reduced numbers, GCs can properly differentiate and mature in the absence of COUP-TFI, and the DG acquires an almost normal shape although smaller in size. This suggests that after exiting the cell cycle, the differentiation capability of a COUP-TFI-deficient cell is not altered, and that the major function of COUP-TFI is to temporally maintain the progenitor pool in a proliferative state.

On the other hand, COUP-TFI controls the behaviour of migratory progenitors along the DMS at prenatal stages and

Development (2017) 144, 2045-2058 doi:10.1242/dev.139949

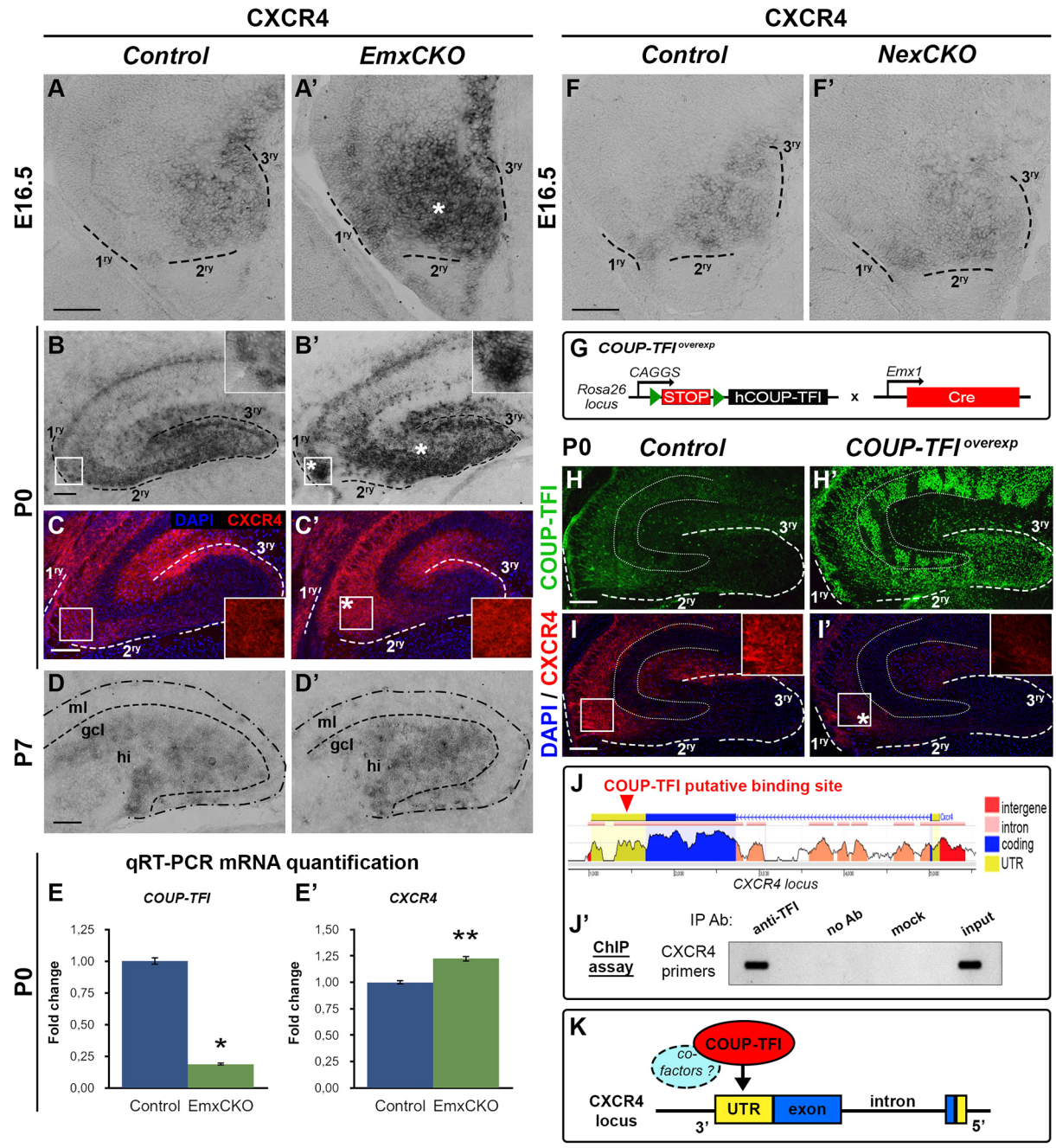

Fig. 8. Altered *Cxcr4* expression after COUP-TFI loss and gain of function in mitotic cells. (A-B′,D,D′) *In situ* hybridization of *Cxcr4* transcript in control and *EmxCKO* DG at the indicated ages. Asterisks and insets in A′ and B′ show an upregulation of *Cxcr4* in *EmxCKO*. (C,C′) Cxcr4 protein expression in P0 control and *EmxCKO* hippocampi. (E,E′) mRNA quantification by qRT-PCR of *COUP-TFI* and *Cxcr4* in control and *EmxCKO*. (F,F′) *In situ* hybridization of *Cxcr4* in E16.5 control and *NexCKO* DG. (G-I′) COUP-TFI overexpression strategy (G) and immunofluorescence of COUP-TFI (H,H′) and Cxcr4 (I,I′) in control and *COUP-TFI*^{overexp} P0 hippocampi. Asterisk and insets indicate Cxcr4 downregulation. (J) Snapshot from ECR browser showing a conserved COUP-TFI putative binding site (red arrowhead) within the *Cxcr4* locus (3′UTR). (J′) ChIP from P0 wild-type hippocampi indicating that COUP-TFI binds this site with strong affinity. A 'no antibody' (no Ab) and a 'mock' (no template) immunoprecipitation are used as negative controls. (K) Schematics of the possible interaction between COUP-TFI protein and the *Cxcr4* locus. gcl, GC layer; hi, hilus; ml, molecular layer. Scale bars: 100 µm.

postnatally, within the hilus and GCL. In its absence, migrating progenitors undertake abnormal paths and form aggregates of cells that will differentiate *in loco* instead of reaching their target destinations (summarized in Fig. 10). This, together with increased apoptosis and a reduced progenitor pool, will strongly affect the growth and morphogenesis of the postnatal DG. Accordingly, the upper blade, where the earliest-born GCs are located, is more affected than the lower blade, in line with early migratory impairments. Even during the late outside-in transgranular radial migration, COUP-TFI-deficient cells are abnormally positioned within the GCL, leading to impairments in the distribution and proliferative capacity of SGZ cells. Very mild defects are observed in mutant differentiating GCs (Fig. 10), indicating that COUP-TFI acts primarily within the progenitor DG population. We also confirmed a stronger defect in the septal rather than temporal pole of COUP-TFI *EmxCKO* mutants, which is in agreement with the

Development (2017) 144, 2045-2058 doi:10.1242/dev.139949

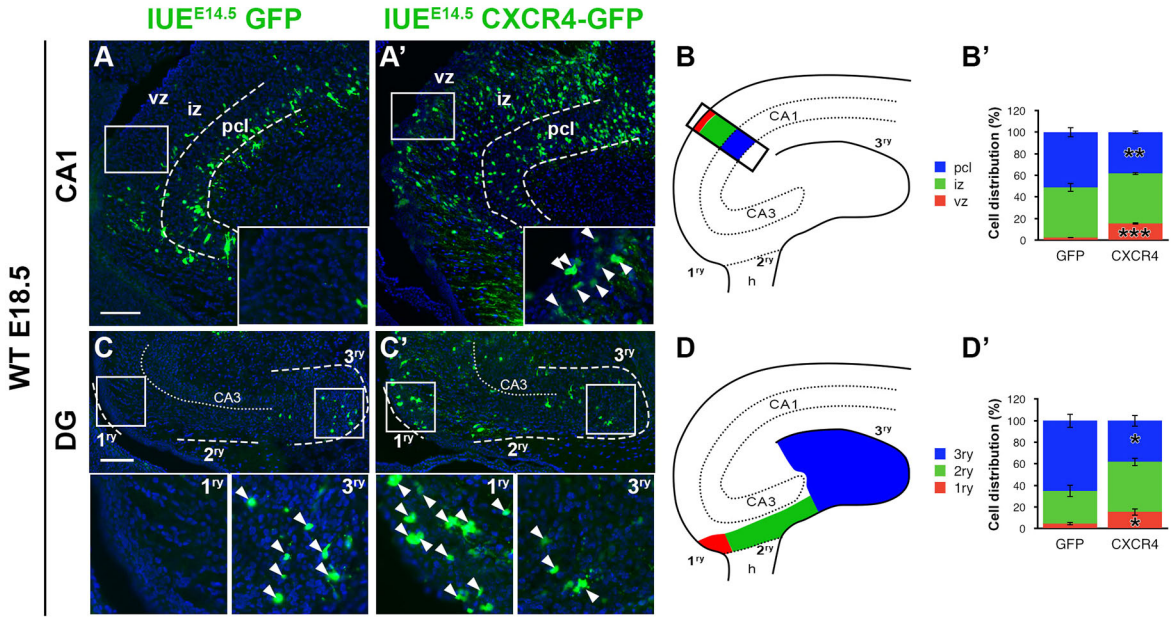

Fig. 9. Overexpressing Cxcr4 in hippocampal cells delays their migration. *In utero* electroporation (IUE) of wild-type hippocampi at E14.5 with *pCIG2-IRES-GFP* (A-C) or *pCIG2-Cxcr4-IRES-GFP* (A′-C′) plasmids. (A-B′) Electroporated (GFP$^+$) cells in the E18.5 CA1 region with magnification in insets (A,A′). B delineates the CA1 counting regions and B′ depicts the GFP$^+$ cell distribution. (C-D′) Electroporated (GFP$^+$) cells in the E18.5 DG matrices with 1ry and 3ry magnifications in insets (C,C′). D delineates the DG counting regions and D′ depicts GFP$^+$ cell distribution. iz, intermediate zone; pcl, pyramidal cell layer; vz, ventricular zone. Arrowheads in insets point to GFP$^+$ cells. Scale bars: 100 µm. *P≤0.05; **P≤0.01; ***P≤0.001.

severe septal hippocampal growth defect described in adult mutants (Flore et al., 2017).

Increased or decreased Cxcr4 expression levels affect cell migration

Several studies using *Cxcl12*- and *Cxcr4*-deficient animals have revealed major functions for these molecules in the prenatal development of the DG (Bagri et al., 2002; Lu et al., 2002). *Cxcr4* is mainly expressed in rapidly dividing granule progenitors and precursors, and in immature GCs (Berger et al., 2007). In *Cxcr4*-deficient animals, progenitors in the DMS and DG are markedly decreased and differentiate prematurely, and postmitotic cells are found ectopically along the migratory route (Bagri et al., 2002; Lu et al., 2002). This phenotype is also partially reproduced in *Tbr2* mutant mice, in which *Cxcr4* expression levels are strongly decreased (Hodge et al., 2013), confirming that Cxcl12/Cxcr4 signalling is mainly required during early phases of DG development. In this study, we show by two independent methods that abnormally high levels of Cxcr4 also lead to delayed aberrant migration, suggesting that altered receptor expression can affect the response of these cells to normal hippocampal Cxcl12 signalling. In addition, Cxcr4 and GFAP expression significantly overlap between P3 and P8 during the reorganization of the hilus and in the forming GCL, indicating additional potential roles for Cxcr4 in the laminar organization of the DG during the first two postnatal weeks (Berger et al., 2007). Aberrant migration, abnormal radial scaffolding and premature neurogenesis are found in COUP-TFI mutant DG (Fig. 10), similar to mice devoid of Cxcl12, Cxcr4 or Tbr2 (Hodge et al., 2013; Li et al., 2009; Lu et al., 2002). Thus, our data suggest that, in progenitor cells, COUP-TFI controls the size and migration of the dentate progenitor pool by normally repressing *Cxcr4* expression, and reveals that multiple transcriptions factors are required to properly maintain precise levels of the receptor Cxcr4 in DG progenitors during development.

COUP-TFI acts differently during cortical pyramidal and granule cell neurogenesis

COUP-TFI is well recognized as a key transcriptional regulator in areal and laminar organisation of neocortical development through its control of the radial migration of late-born neurons and its specification of sensory pyramidal neuron fate primarily in early postmitotic cells (Alfano et al., 2011, 2014a,b). Here, we show that COUP-TFI acts predominantly in progenitor cells by regulating the size of the progenitor pool and allowing proper migration of GC precursors. How can we explain this discrepancy in the mitotic versus postmitotic role of COUP-TFI between DG and neocortical development?

DG morphogenesis starts around mid-gestation in the mouse and substantially differs from other cortical regions. In the neocortex, neurogenesis and cell migration are two distinct processes occurring at different times and in distinct radial compartments (Florio and Huttner, 2014), whereas DG progenitors proliferate and produce new neurons as they migrate to the hilar region, where they continue their GC production until they reach their final residence in the SGZ (Hevner, 2016; Li and Pleasure, 2005). Thus, cell migration is prolonged in the DG when compared with cortical development, and cell proliferation and migration are two highly linked processes in the DG, whereas in the neocortex migrating cells do not proliferate. Thus, it is plausible that proliferation and migration closely influence each other in the DG and/or are controlled by similar mechanisms. In addition, as progenitors divide while migrating, they are continuously exposed to signalling molecules along their paths. COUP-TFI has been shown to be an important regulator of cell migration *in vivo* during forebrain development (Alfano et al., 2011; Touzot et al., 2016; Tripodi et al., 2004; Zhou et al., 2015), but also *in vitro* and in cancerous cells (Adam et al., 2000; Boudot et al., 2014; Le Dily et al., 2008). Here, we show that it modulates the correct expression levels of the chemokine receptor gene *Cxcr4* during GC neurogenesis and migration. Thus, by

Development (2017) 144, 2045-2058 doi:10.1242/dev.139949

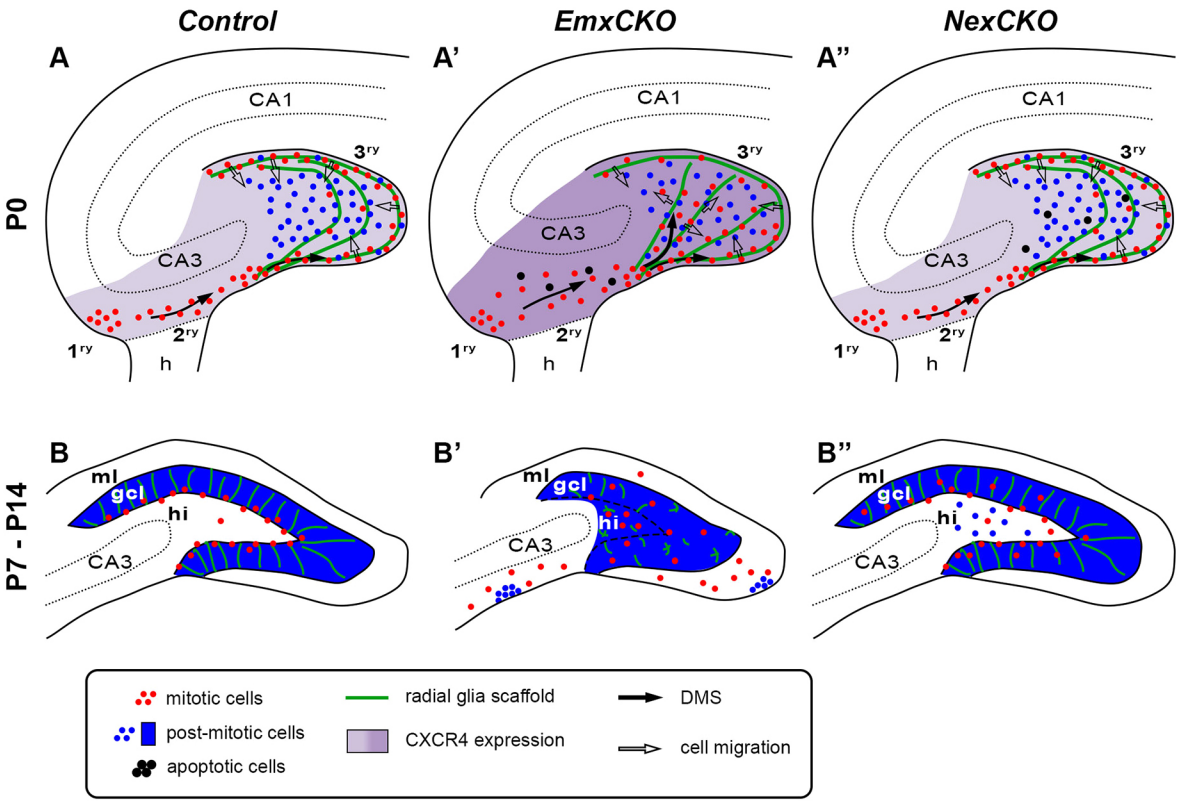

Fig. 10. Summary of the DG defects observed in *EmxCKO* and *NexCKO* mutant mice. Overview of the different phenotypes observed in *EmxCKO* and *NexCKO* at birth (A-A″) and at postnatal stages (B-B″). (A) GC progenitors and IPC (red cells) migrate through the DMS in the 2ry matrix and along the pial surface (black arrows) following the primary radial glia scaffold (green lines), and towards the 3ry matrix where postmitotic cells accumulate (blue cells). Empty arrows indicate outside-in migrating GCs. (A′) In *EmxCKO*, migrating cells are disorganized and follow abnormal migratory paths (black arrows) along the 2ry matrix and trans-hilar scaffolding (green lines). *Cxcr4* expression is upregulated in these mutants (dark purple). (A″) *NexCKO* show no or only mild defects of migrating GCs and scaffolding. Apoptotic cells are represented as black dots in the 2ry matrix of *EmxCKO* and 3ry matrix of *NexCKO*. (B) At P7, mitotic cells are gathered at the border between hilus and GC layer, and establish the future SGZ at P14. (B′) In *EmxCKO*, mitotic cells accumulate in the hilus and ml, encounter disorganized scaffolding (green lines), form ectopic clusters of postmitotic cells (blue dots) and fail to generate a proper laminar organization (blue area). (B″) *NexCKO* mutants show a mild and transient laminar defect of GCs, rescued at later stages. DMS, dentate migratory stream; gcl, GC layer; h, hem; hi, hilus; ml, molecular layer.

maintaining a key role in cell migration, COUP-TFI is able to play different functions in distinct cell types according to the biological process in which it is implicated.

MATERIALS AND METHODS

Animals

Generation of *COUP-TFI* conditional and overexpressing mice, as well as the *Thy1-eYFP-H* line have been previously described (Alfano et al., 2014b; Armentano et al., 2007; Harb et al., 2016). Midday on the day of vaginal plug formation was considered as embryonic day 0.5 (E0.5). All experiments were conducted according to French ethical regulations and received the approval from our local ethics committee (CIEPAL NCE/2014-209).

Immunohistochemistry and immunofluorescence

Postnatal mice were perfused with 4% paraformaldehyde (PFA) in PBS and post-fixed in 4% PFA at 4°C, for either 2 h for immunofluorescence or immunohistochemitry, or overnight for *in situ* hybridization experiments. Cryosections (16 µm) were processed for immunofluorescence or immunohistochemistry, as previously described (Alfano et al., 2014b) by overnight incubation at 4°C with the primary antibodies, followed by 2 h at room temperature with secondary antibodies (Table S1). Immunohistochemistry slides followed the standard avidin-biotin complex reaction procedure (Vector Laboratories), and staining was revealed using DAB Peroxidase Substrate (Vector) following the manufacturer's instructions.

In situ hybridization

Cxcr4 and *Cxcl12* antisense RNA probes were labelled using a DIG-RNA Labelling Kit (Roche). *In situ* hybridizations were carried out on 16 µm cryosections as previously described (Alfano et al., 2014b).

Birth-dating

Timed-pregnant females were injected intraperitoneally with 200 µl (2.5 g/ml) of EdU (FisherScientific) and revealed by using the EdU Click-It Alexa Fluor 647 kit (FisherScientific). Slides were stained for immunofluorescence with the appropriate antibodies just prior to EdU revelation. For adult neurogenesis, BrdU (Sigma) was administered intraperitoneally to 2-month-old mice at 100 g/kg for six consecutive days and sacrificed the day after.

Nissl staining

Cryosections (16 µm) were post-fixed in 4% PFA for 10 min and incubated in the staining solution (0.025% thionin, 0.025% Cresyl Violet, 100 mM sodium acetate, 8 mM acetic acid, in deionized H_2O) for 5 min at room temperature. Visualization was carried out in the de-coloration solution (80% ethanol, 20% deionized H_2O and few drops of acetic acid). Vibratome sections (50 µm) from 2-month-old adult mice were processed as previously described (Flore et al., 2017).

Imaging

Pictures were taken using an epifluorescence microscope (Zeiss Imager.M2) or a confocal microscope (Zeiss 710) for immunofluorescence and with a

Development (2017) 144, 2045-2058 doi:10.1242/dev.139949

bright-field microscope (Leica DM6000B) equipped with a colour camera for immunohistochemistry, *in situ* hybridization and Nissl staining.

Quantitative reverse-transcriptase PCR

Total RNA (1 mg) was reverse-transcribed using Superscript III First-Strand Synthesis System for RT-PCR (Invitrogen). Amplified cDNA was quantified using KAPA SYBR FAST Master Mix (Kapa Biosystems) on a LightCycler II 480 (Roche) (see supplementary Materials and Methods for further details).

Chromatin immunoprecipitation

Hippocampi were dissected from 14 wild-type mice at P0 and chromatin immunoprecipitation was performed as previously described (Harb et al., 2016). Anti-COUP-TFI antibody (Alfano et al., 2011) was used for immunoprecipitation. Binding of COUP-TFI to the *Cxcr4* sequence was tested by PCR amplification using primers designed to recognize the putative binding site (Table S2).

In utero electroporation

In utero electroporation was performed on E14.5 hippocampal neuroepithelium as previously described (Pacary and Guillemot, 2014) by trying to target the DGN and using the following parameters: four 40 V pulses, P(on) 50 ms, P(off) 1 s. The following plasmids were used: *pCIG2-IRES*-GFP (Heng et al., 2008) (n=7) or *pCIG2-Cxcr4-IRES-GFP* (n=9). The latter one was produced by cloning a PCR-amplified *Cxcr4* DNA sequence into the *Eco*RI and *Xma*I sites of the *pCIG2-IRES-GFP* plasmid. Brains were collected at E18.5 and processed as for immunofluorescence.

Quantification and statistical analysis

DG volumes of at least n=3 *EmxCKO* or *NexCKO* were calculated and compared with their respective littermate controls. The volume of the adult DG and/or hippocampus was evaluated with the NIH ImageJ Software and analysed by a two-way ANOVA for repeated measures, and Duncan's post-hoc test. Cell counts were performed on at least three consecutive rostral sections for each analysed brain using the counting tool of Adobe Photoshop CS6. A spreadsheet software and a two-tailed paired Student's t-test were used to analyse statistical significance between mutant and their controls (*P<0,05; **P<0,01; ***P<0,001). All graphs represent mean+s.e.m. A detailed description can be found in supplementary Materials and Methods.

Acknowledgements

We thank K. R. Jones for the *Emx1-Cre,* K. A. Nave for the *Nex-Cre* and M. Tsai for the *CAGGS-loxP-STOP-loxP-hCOUP-TFI* mouse lines, as well as M. C. Tiveron for the *Cxcl12* and *Cxcr4* plasmids. We are also grateful to Eya Setti for her technical help, to S. De Marchis and S. Bonzano for their suggestions on the manuscript, and to the whole Studer lab for fruitful discussions.

Competing interests

The authors declare no competing or financial interests.

Author contributions

Conceptualization: J.P., G.F., M.B., M.S.; Methodology: J.P., G.F., M.B., M.S.; Validation: J.P., G.F., M.B.; Formal analysis: J.P., G.F., M.B., M.S.; Investigation: J.P., G.F., M.B.; Resources: J.P., G.F.; Data curation: J.P., G.F., M.B., M.S.; Writing - original draft: J.P., M.S.; Writing - review & editing: J.P., G.F., M.B., M.S.; Supervision: M.S.; Project administration: M.S.; Funding acquisition: M.S.

Funding

This work was supported by the Agence Nationale de la Recherche (ANR) (ANR-13-BSV4-0011), by the Fondation Jérôme Lejeune (R13098AA) and by the Fédération pour la Recherche sur le Cerveau (FRC) (R14032AA) to M.S., and by the Agence Nationale de la Recherche through the 'Investments for the Future' LABEX SIGNALIFE (ANR-11-LABX-0028-01). J.P. was supported by a personal fellowship from the Région PACA, and G.F. by fellowships issued from the Fondazione Telethon (TCP04006) and Ministerial European grants (PON01_02342).

Supplementary information

Supplementary information available online at
http://dev.biologists.org/lookup/doi/10.1242/dev.139949.supplemental

References

Adam, F., Sourisseau, T., Métivier, R., Le Page, Y., Desbois, C., Michel, D. and Salbert, G. (2000). COUP-TFI (chicken ovalbumin upstream promoter-transcription factor I) regulates cell migration and axogenesis in differentiating P19 embryonal carcinoma cells. *Mol. Endocrinol.* **14**, 1918-1933.

Alfano, C., Viola, L., Heng, J. I.-T., Pirozzi, M., Clarkson, M., Flore, G., De Maio, A., Schedl, A., Guillemot, F. and Studer, M. (2011). COUP-TFI promotes radial migration and proper morphology of callosal projection neurons by repressing Rnd2 expression. *Development* **138**, 4685-4697.

Alfano, C., Magrinelli, E., Harb, K. and Studer, M. (2014a). The nuclear receptors COUP-TF: a long-lasting experience in forebrain assembly. *Cell. Mol. Life Sci.* **71**, 43-62.

Alfano, C., Magrinelli, E., Harb, K., Hevner, R. F. and Studer, M. (2014b). Postmitotic control of sensory area specification during neocortical development. *Nat. Commun.* **5**, 5632.

Altman, J. and Bayer, S. A. (1990a). Migration and distribution of two populations of hippocampal granule cell precursors during the perinatal and postnatal periods. *J. Comp. Neurol.* **301**, 365-381.

Altman, J. and Bayer, S. A. (1990b). Mosaic organization of the hippocampal neuroepithelium and the multiple germinal sources of dentate granule cells. *J. Comp. Neurol.* **301**, 325-342.

Altman, J. and Bayer, S. A. (1990c). Prolonged sojourn of developing pyramidal cells in the intermediate zone of the hippocampus and their settling in the stratum pyramidale. *J. Comp. Neurol.* **301**, 343-364.

Altman, J. and Das, G. D. (1965). Autoradiographic and histological evidence of postnatal hippocampal neurogenesis in rats. *J. Comp. Neurol.* **124**, 319-335.

Armentano, M., Chou, S.-J., Tomassy, G. S., Leingärtner, A., O'Leary, D. D. M. and Studer, M. (2007). COUP-TFI regulates the balance of cortical patterning between frontal/motor and sensory areas. *Nat. Neurosci.* **10**, 1277-1286.

Bagri, A., Gurney, T., He, X., Zou, Y. R., Littman, D. R., Tessier-Lavigne, M. and Pleasure, S. J. (2002). The chemokine SDF1 regulates migration of dentate granule cells. *Development* **129**, 4249-4260.

Berger, O., Li, G., Han, S.-M., Paredes, M. and Pleasure, S. J. (2007). Expression of SDF-1 and CXCR4 during reorganization of the postnatal dentate gyrus. *Dev. Neurosci.* **29**, 48-58.

Boudot, A., Kerdivel, G., Lecomte, S., Flouriot, G., Desille, M., Godey, F., Leveque, J., Tas, P., Le Dréan, Y. and Pakdel, F. (2014). COUP-TFI modifies CXCL12 and CXCR4 expression by activating EGF signaling and stimulates breast cancer cell migration. *BMC Cancer* **14**, 407.

Brunne, B., Zhao, S., Derouiche, A., Herz, J., May, P., Frotscher, M. and Bock, H. H. (2010). Origin, maturation, and astroglial transformation of secondary radial glial cells in the developing dentate gyrus. *Glia* **58**, 1553-1569.

Cowan, W. M., Stanfield, B. B. and Kishi, K. (1980). The development of the dentate gyrus. *Curr. Top. Dev. Biol.* **15**, 103-157.

Eckenhoff, M. F. and Rakic, P. (1988). Nature and fate of proliferative cells in the hippocampal dentate gyrus during the life span of the rhesus monkey. *J. Neurosci.* **8**, 2729-2747.

Englund, C., Fink, A., Lau, C., Pham, D., Daza, R. A., Bulfone, A., Kowalczyk, T. and Hevner, R. F. (2005). Pax6, Tbr2, and Tbr1 are expressed sequentially by radial glia, intermediate progenitor cells, and postmitotic neurons in developing neocortex. *J. Neurosci.* **25**, 247-251.

Flore, G., Di Ruberto, G., Parisot, J., Sannino, S., Russo, F., Illingworth, E. A., Studer, M. and De Leonibus, E. (2017). Gradient COUP-TFI expression is required for functional organization of the hippocampal septo-temporal longitudinal axis. *Cereb. Cortex.* **27**, 1629-1643.

Florio, M. and Huttner, W. B. (2014). Neural progenitors, neurogenesis and the evolution of the neocortex. *Development* **141**, 2182-2194.

Galceran, J., Miyashita-Lin, E. M., Devaney, E., Rubenstein, J. L. and Grosschedl, R. (2000). Hippocampus development and generation of dentate gyrus granule cells is regulated by LEF1. *Development* **127**, 469-482.

Galeeva, A., Treuter, E., Tomarev, S. and Pelto-Huikko, M. (2007). A prospero-related homeobox gene Prox-1 is expressed during postnatal brain development as well as in the adult rodent brain. *Neuroscience* **146**, 604-616.

Galichet, C., Guillemot, F. and Parras, C. M. (2008). Neurogenin 2 has an essential role in development of the dentate gyrus. *Development* **135**, 2031-2041.

Goebbels, S., Bormuth, I., Bode, U., Hermanson, O., Schwab, M. H. and Nave, K.-A. (2006). Genetic targeting of principal neurons in neocortex and hippocampus of NEX-Cre mice. *Genesis* **44**, 611-621.

Gotz, M., Stoykova, A. and Gruss, P. (1998). Pax6 controls radial glia differentiation in the cerebral cortex. *Neuron* **21**, 1031-1044.

Harb, K., Magrinelli, E., Nicolas, C. S., Lukianets, N., Frangeul, L., Pietri, M., Sun, T., Sandoz, G., Grammont, F., Jabaudon, D. et al. (2016). Area-specific development of distinct projection neuron subclasses is regulated by postnatal epigenetic modifications. *Elife* **5**, e09531.

Heng, J. I.-T., Nguyen, L., Castro, D. S., Zimmer, C., Wildner, H., Armant, O., Skowronska-Krawczyk, D., Bedogni, F., Matter, J.-M., Hevner, R. et al. (2008). Neurogenin 2 controls cortical neuron migration through regulation of Rnd2. *Nature* **455**, 114-118.

Hevner, R. F. (2016). Evolution of the mammalian dentate gyrus. *J. Comp. Neurol.* **524**, 578-594.

Development (2017) 144, 2045-2058 doi:10.1242/dev.139949

Hodge, R. D., Nelson, B. R., Kahoud, R. J., Yang, R., Mussar, K. E., Reiner, S. L. and Hevner, R. F. (2012). Tbr2 is essential for hippocampal lineage progression from neural stem cells to intermediate progenitors and neurons. *J. Neurosci.* **32**, 6275-6287.

Hodge, R. D., Garcia, A. J., III, Elsen, G. E., Nelson, B. R., Mussar, K. E., Reiner, S. L., Ramirez, J.-M. and Hevner, R. F. (2013). Tbr2 expression in Cajal-Retzius cells and intermediate neuronal progenitors is required for morphogenesis of the dentate gyrus. *J. Neurosci.* **33**, 4165-4180.

Iwano, T., Masuda, A., Kiyonari, H., Enomoto, H. and Matsuzaki, F. (2012). Prox1 postmitotically defines dentate gyrus cells by specifying granule cell identity over CA3 pyramidal cell fate in the hippocampus. *Development* **139**, 3051-3062.

Lavado, A. and Oliver, G. (2007). Prox1 expression patterns in the developing and adult murine brain. *Dev. Dyn.* **236**, 518-524.

Lavado, A., Lagutin, O. V., Chow, L. M. L., Baker, S. J. and Oliver, G. (2010). Prox1 is required for granule cell maturation and intermediate progenitor maintenance during brain neurogenesis. *PLoS Biol.* **8**, e1000460.

Le Dily, F., Métivier, R., Guéguen, M.-M., Le Péron, C., Flouriot, G., Tas, P. and Pakdel, F. (2008). COUP-TFI modulates estrogen signaling and influences proliferation, survival and migration of breast cancer cells. *Breast Cancer Res. Treat.* **110**, 69-83.

Li, G. and Pleasure, S. J. (2005). Morphogenesis of the dentate gyrus: what we are learning from mouse mutants. *Dev. Neurosci.* **27**, 93-99.

Li, G., Kataoka, H., Coughlin, S. R. and Pleasure, S. J. (2009). Identification of a transient subpial neurogenic zone in the developing dentate gyrus and its regulation by Cxcl12 and reelin signaling. *Development* **136**, 327-335.

Loots, G. and Ovcharenko, I. (2007). ECRbase: database of evolutionary conserved regions, promoters, and transcription factor binding sites in vertebrate genomes. *Bioinformatics* **23**, 122-124.

Lu, M., Grove, E. A. and Miller, R. J. (2002). Abnormal development of the hippocampal dentate gyrus in mice lacking the CXCR4 chemokine receptor. *Proc. Natl. Acad. Sci. USA* **99**, 7090-7095.

Muramatsu, R., Ikegaya, Y., Matsuki, N. and Koyama, R. (2007). Neonatally born granule cells numerically dominate adult mice dentate gyrus. *Neuroscience* **148**, 593-598.

Nowakowski, R. S. and Rakic, P. (1981). The site of origin and route and rate of migration of neurons to the hippocampal region of the rhesus monkey. *J. Comp. Neurol.* **196**, 129-154.

Pacary, E. and Guillemot, F. (2014). In utero electroporation to study mouse brain development. *Methods Mol. Biol.* **1082**, 285-293.

Pleasure, S. J., Collins, A. E. and Lowenstein, D. H. (2000). Unique expression patterns of cell fate molecules delineate sequential stages of dentate gyrus development. *J. Neurosci.* **20**, 6095-6105.

Porter, A. G. and Janicke, R. U. (1999). Emerging roles of caspase-3 in apoptosis. *Cell Death Differ.* **6**, 99-104.

Quandt, K., Frech, K., Karas, H., Wingender, E. and Werner, T. (1995). MatInd and MatInspector: new fast and versatile tools for detection of consensus matches in nucleotide sequence data. *Nucleic Acids Res.* **23**, 4878-4884.

Rakic, P. and Nowakowski, R. S. (1981). The time of origin of neurons in the hippocampal region of the rhesus monkey. *J. Comp. Neurol.* **196**, 99-128.

Roybon, L., Hjalt, T., Stott, S., Guillemot, F., Li, J.-Y. and Brundin, P. (2009). Neurogenin2 directs granule neuroblast production and amplification while NeuroD1 specifies neuronal fate during hippocampal neurogenesis. *PLoS ONE* **4**, e4779.

Sugiyama, T., Osumi, N. and Katsuyama, Y. (2013). The germinal matrices in the developing dentate gyrus are composed of neuronal progenitors at distinct differentiation stages. *Dev. Dyn.* **242**, 1442-1453.

Touzot, A., Ruiz-Reig, N., Vitalis, T. and Studer, M. (2016). Molecular control of two novel migratory paths for CGE-derived interneurons in the developing mouse brain. *Development* **143**, 1753-1765.

Tripodi, M., Filosa, A., Armentano, M. and Studer, M. (2004). The COUP-TF nuclear receptors regulate cell migration in the mammalian basal forebrain. *Development* **131**, 6119-6129.

Urban, N. and Guillemot, F. (2014). Neurogenesis in the embryonic and adult brain: same regulators, different roles. *Front. Cell. Neurosci.* **8**, 396.

Zhou, X., Liu, F., Tian, M., Xu, Z., Liang, Q., Wang, C., Li, J., Liu, Z., Tang, K., He, M. et al. (2015). Transcription factors COUP-TFI and COUP-TFII are required for the production of granule cells in the mouse olfactory bulb. *Development* **142**, 1593-1605.

SUPPLEMENTARY FIGURES

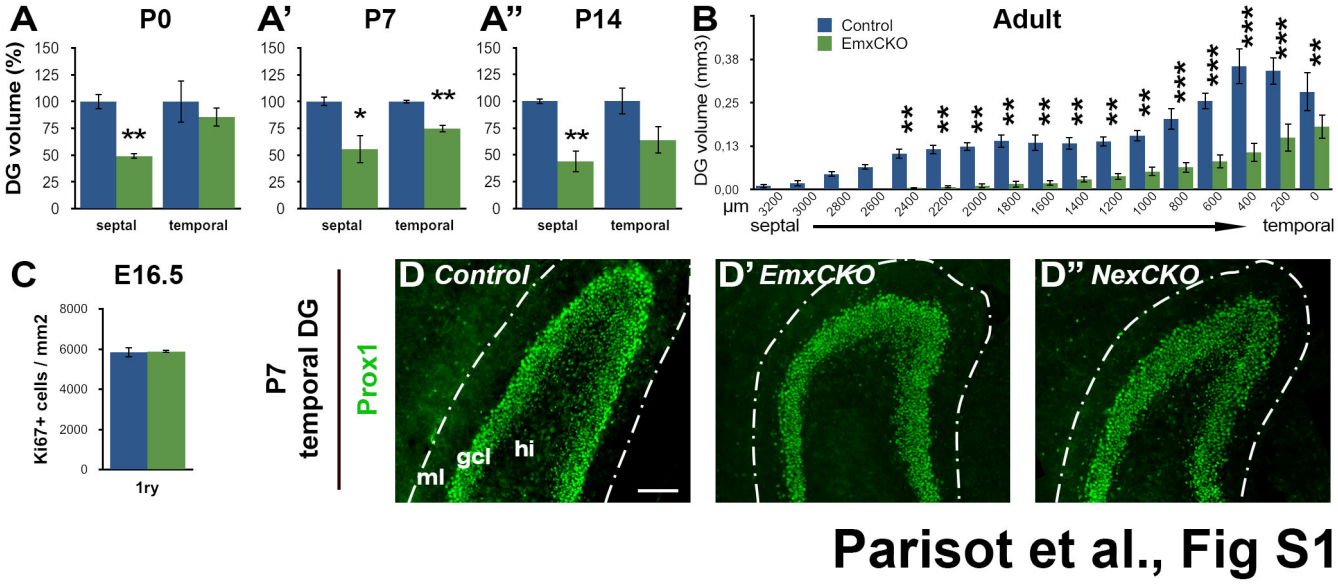

Figure S1. COUP-TFI loss in progenitors affects mainly the septal dentate gyrus (DG). **(A-A")** Quantification of septal and temporal DG volumes in control and *EmxCKO* mutants, set up to 100% of controls at P0 (A), P7 (A') and P14 (A"), shows a stronger volume decrease in the septal than temporal pole. **(B)** Septo-temporal distribution of DG volume in the adult. **(C)** No changes in the density of Ki67+ cycling cells in the temporal 1ry matrix of *EmxCKO* DG at E16.5. **(D-D")** Temporal DG lamination labelled by Prox1 in P7 *EmxCKO* and *NexCKO* DGs indicates no particular accumulation of Prox1+ cells in the hilus (as instead observed in the septal pole, see Fig. 5E'). *gcl: granule cell layer; hi: hilus; ml: molecular layer. Scale bar: 100µm. *p≤0,05; **p≤0,01; ***p≤0,001.*

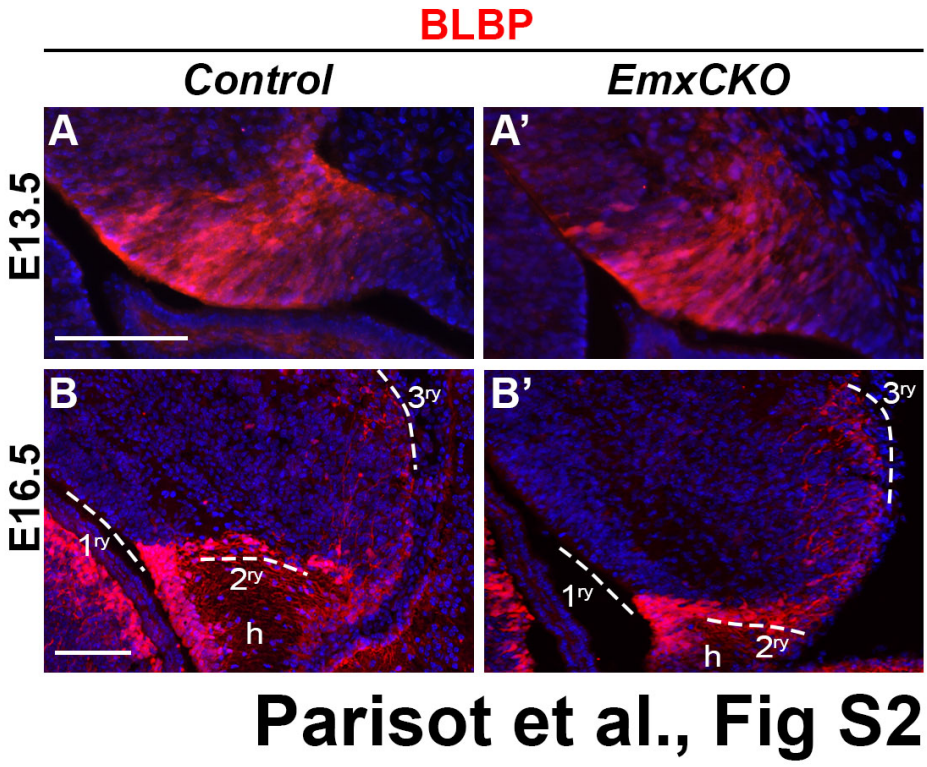

Figure S2. No obvious defects in the embryonic scaffold in the absence of COUP-TFI in progenitors. (A-A') BLBP immunostaining on the primordial hippocampus in E13.5 control and *EmxCKO* embryos. **(B-B')** BLBP immunostaining on the developing DG in E16.5 control and *EmxCKO* embryos. At both developmental stages, BLBP+ cells are mainly located around the cortical hem with few fibres extending to the 3^{ry} matrix in controls and *EmxCKO* embryos. *h: cortical hem. Scale bar: 100µm.*

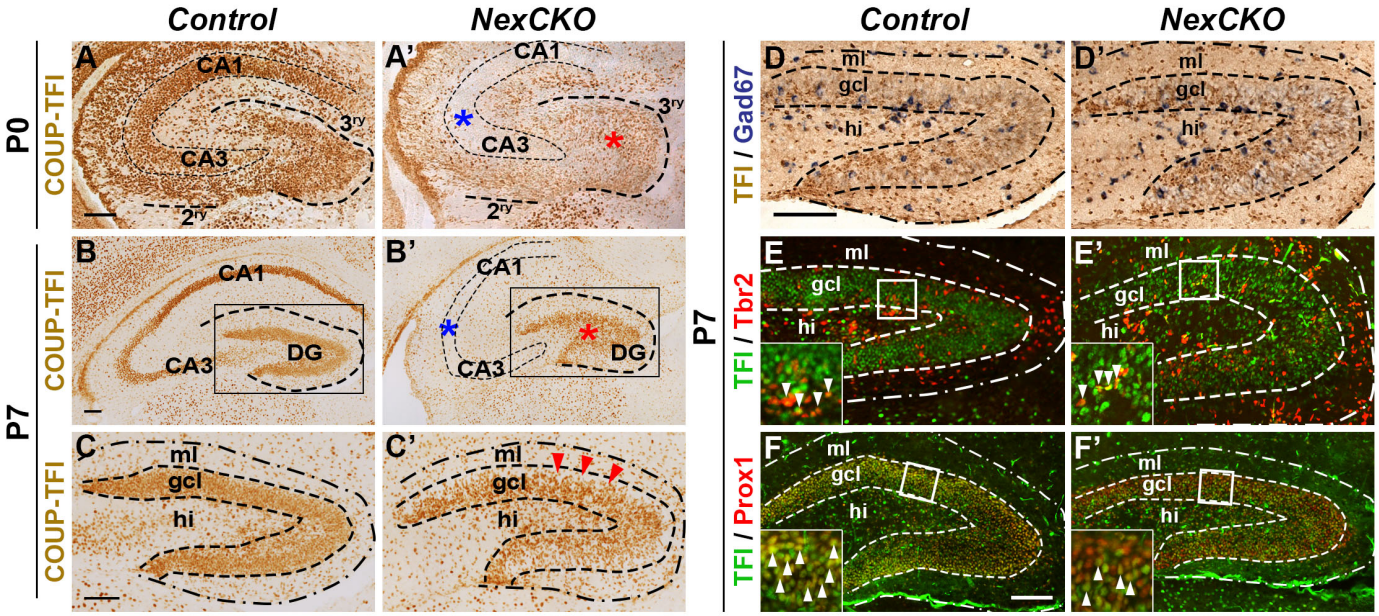

Parisot et al., Fig S3

Figure S3. COUP-TFI is depleted in late postmitotic granule cells of the *NexCKO* dentate gyrus (DG). (A-C') COUP-TFI immunostaining in control and *NexCKO* post-natal hippocampal coronal sections at P0 (A-A') and P7 (B-C'). Blue asterisks in A'-B' support the expected loss of COUP-TFI expression in postmitotic pyramidal cells of CA1-3, whereas red asterisks highlight decrease of COUP-TFI-expressing cells in the DG. (C-C') High magnification views of the boxes in B-B'. Red arrowheads in C' indicate complete loss of COUP-TFI protein in the external one-third of the GC layer (gcl), where more mature GCs are located, whereas expression is only slightly decreased in the inner two-third where progenitors and precursors are still maintained. **(D-D')** Double staining for COUP-TFI protein (IHC) and *Gad67* expression (ISH) in P7 control and mutant DGs. The number and distribution of COUP-TFI+ interneurons appear similar to control in *NexCKO* DGs. **(E-F')** Co-expression of COUP-TFI in Tbr2+ (E-E') and Prox1+ cells (F-F') in control and *NexCKO* DGs at P7. Arrowheads in insets indicate double-labelled cells and indicate that COUP-TFI is still expressed in Tbr2+ IPC, and in some Prox1+ granule precursors. *gcl: granule cell layer; hi: hilus; ml: molecular layer. Scale bars: 100µm.*

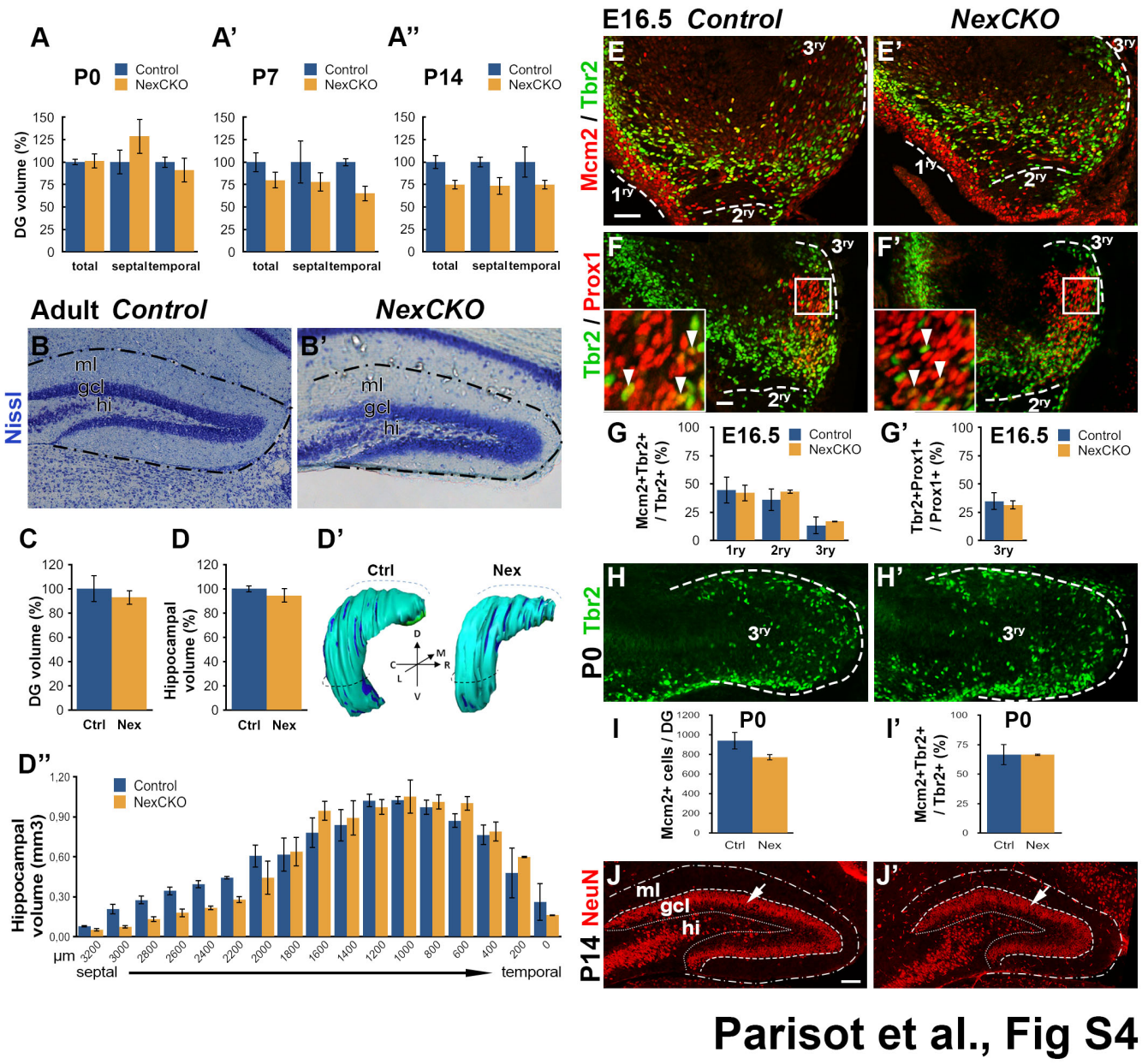

Parisot et al., Fig S4

Figure S4. Loss of COUP-TFI function in postmitotic cells does not affect growth and granule cell differentiation. (A-A") Volume of total, septal and temporal control and *NexCKO* DG at P0, P7 and P14. **(B-C)** Nissl staining of adult septal DG and total DG volume (C) show no significant differences between control and mutants. **(D-D")** Global hippocampal volume is not affected in adult *NexCKO* brains (D). D' represents a 3D reconstruction of control and *NexCKO* hippocampi and D" corresponds to the septo-temporal distribution of hippocampal volume. **(E-F')** Co-expression of Mcm2/Tbr2 and Tbr2/Prox1 in E16.5 control

and *NexCKO* DGs. The amount of Tbr2+ IPC expressing the cell cycle marker Mcm2 (G) and the amount of Prox1+ GCs expressing Tbr2 (G') are not changed between controls and mutant DGs. **(H-H')** Tbr2+ IPCs in P0 *NexCKO* DGs are found in similar number and distribution to controls. **(I-I')** Mitotic Mcm2+ cells are not affected in *NexCKO* DGs (F), nor the proliferative capacity of IPCs (F'). **(J-J')** Expression and distribution of the mature neuronal marker NeuN is found in the external two-third of the granule cell layer (gcl) in control and *NexCKO* DGs. *hi: hilus; ml: molecular layer. Scale bars: 100µm.*

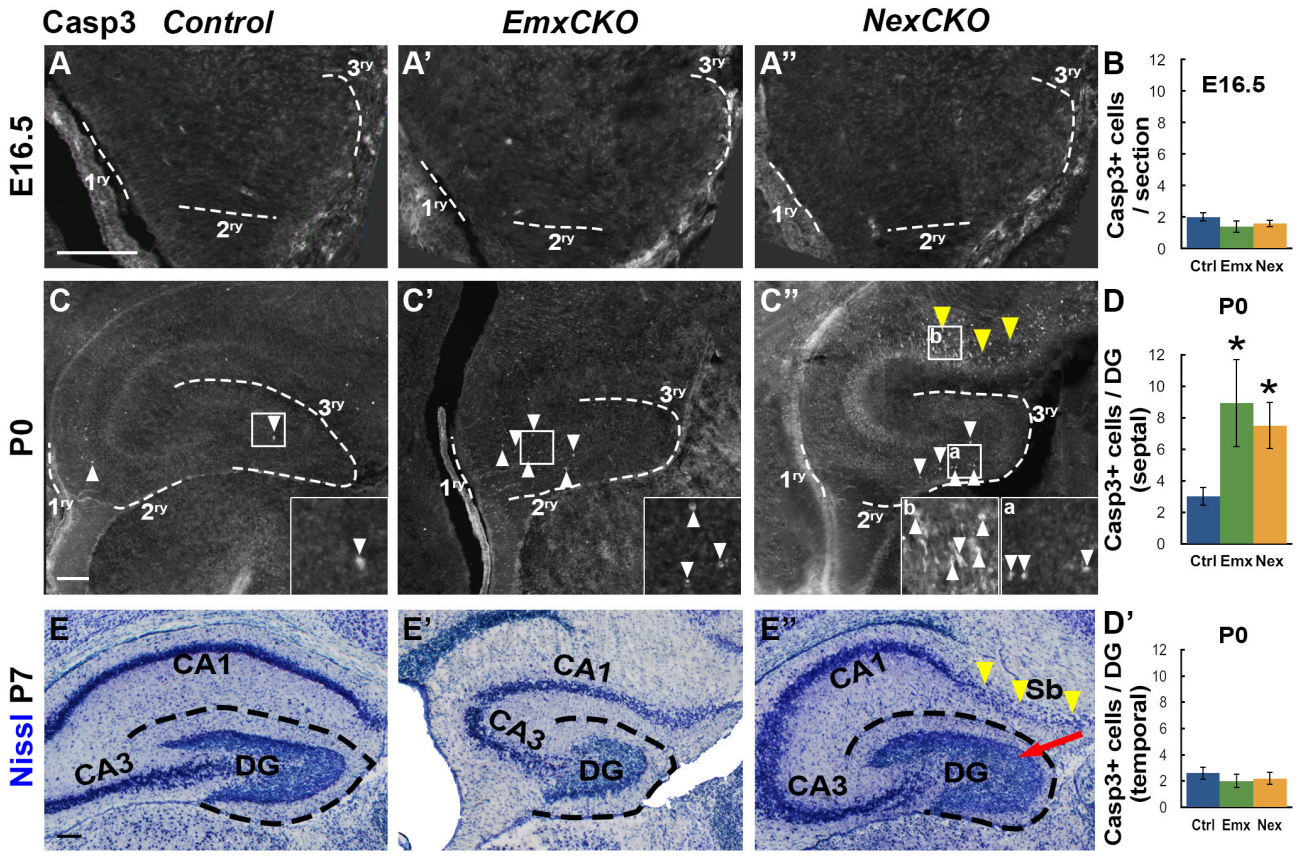

Parisot et al., Fig S5

Figure S5. Increased perinatal cell death in both *EmxCKO* and *NexCKO* dentate gyri. **(A-D)** Immunolabelling of active-Caspase3 in coronal sections of control and *COUP-TFI* mutant DGs to evaluate cell death. No increase in cell death is found at E16.5 in the 3 matrices (A-B). At P0 (C-D), significant increase of Casp3+ cells are detected in both *EmxCKO* and *NexCKO* mutant septal DG (D), whereas no differences are observed in the temporal DG (D'). Cell counts in D-D' encompass all 3 matrices of the DG at P0. White arrowheads in C-C" and their insets point to apoptotic cells in the developing DG, which are located mostly in the 2^{ry} matrix (migratory stream) in *EmxCKO* and 3^{ry} matrix in *NexCKO*. Yellow arrowheads in C" indicate an additional strong increase of Casp3+ dying cells in the subiculum (Sb) of *NexCKO*. **(E-E")** Nissl staining of P7 coronal sections of hippocampi showing cell depletion in the *NexCKO* subiculum (yellow arrowheads), which might partially explain the roundish appearance of *NexCKO* DGs (red arrow). *Scale bars: 100µm. *p≤0,05.*

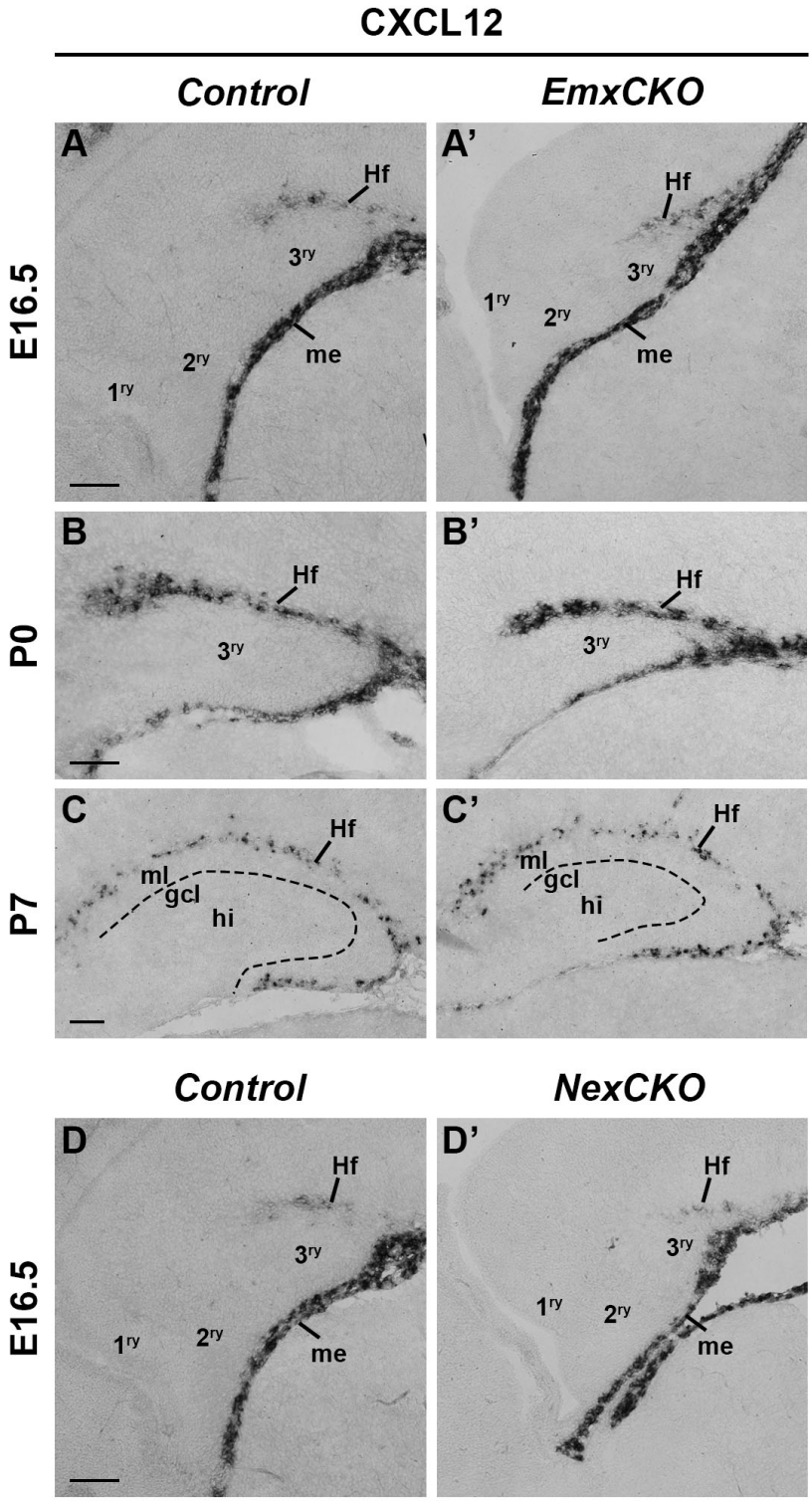

Parisot et al., Fig S6

Figure S6. Normal *CXCL12* mRNA expression in *EmxCKO* and *NexCKO* hippocampi. **(A-C')** *In situ* hybridization (ISH) of *CXCL12* transcripts in control and *EmxCKO* DGs at the indicated ages. **(D-D')** ISH of *CXCL12* in E16.5 control and *NexCKO* DGs. *gcl: GC layer; Hf: hippocampal fissure; hi: hilus; me: meninges; ml: molecular layer. Scale bars: 100µm.*

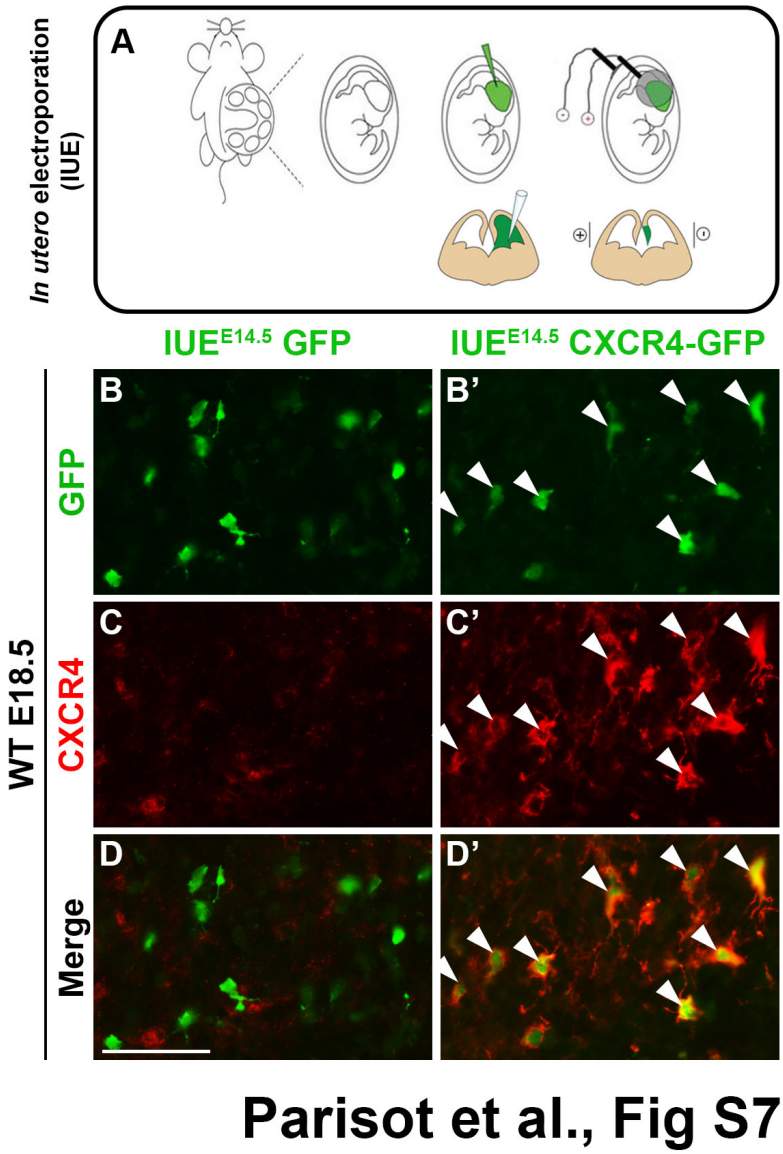

Figure S7. Electroporation of the *pCIG2-CXCR4-IRES-GFP* (CXCR4-GFP) plasmid properly express CXCR4 in GFP+ cells. (A) *In utero* electroporation strategy (images adapted from (Pacary et al., 2012)) to hit the hippocampal neuroepithelium of E14.5-old embryos. **(B-D')** Immunofluorescence for GFP and CXCR4 on E18.5 brains electroporated at E14.5 with *pCIG2-IRES-GFP* (B-D) or *pCIG2-CXCR4-IRES-GFP* (B'-D') plasmids. Pictures are taken in the CA1 region. Cells that express the CXCR4-GFP plasmid effectively overexpress CXCR4 protein (arrowheads). *Scale bar: 50µm*.

SUPPLEMENTARY MATERIALS AND METHODS

Quantitative reverse-transcriptase PCR (qRT-PCR).

Total RNA for qRT–PCR was extracted from fresh P0 hippocampi of at least 4 animals for each genotype using the NucleoSpin RNAII columns (Macherey-Nagel) following manufacturer's instructions. After RNA extraction, RNA quality was assessed with Nanodrop and gel electrophoresis. For each sample, 1mg of total RNA was reverse-transcribed using Superscript III First-Strand Synthesis System for RT–PCR (Invitrogen) following manufacturer's instructions. Amplified cDNA was quantified using KAPA SYBR FAST Master Mix (Kapa Biosystems) on a LigthCycler II 480 (Roche). Amplification take-off values were evaluated using the built-in LightCycler 480 relative quantification analysis function, and relative expression was calculated with the 2 -ΔΔCt method, normalizing with respect to the housekeeping gene ß-Actin. Fold-change variations in the levels of mRNA of interest were expressed as a percentage and normalized against WT levels (set as 100%), and standard errors were obtained from the error propagation formula. Primer sequences are listed in **Table S2**.

Quantification and statistical analysis

Volume measurements were performed using Adobe Photoshop CS6 software on the entire septo-temporal axis of Nissl-stained vibratome sections. The total, septal and temporal DG volumes of at least n=3 *EmxCKO* or *NexCKO* were calculated and compared to their respective littermate controls. The volume of the adult DG and/or hippocampus and its septo-temporal distribution was evaluated on coronal sections with the NIH *ImageJ* Software and analysed by a two-way ANOVA for repeated measures, with genotype as between group measure, and septo-temporal gradient as repeated measure. A Duncan post hoc test was used,

when appropriate, to make direct comparisons. 3D illustrations were obtained as previously described (Flore et al., 2016). Statistical significance between mutants and controls was analyzed using the Dell software *Statistica 10* and the two-tailed paired Student's t-test. Data were normalized, by defining the control value as 100%.

Cell quantification was performed on 3 coronal anatomically matched sections within the septal or temporal hippocampus of at least n=3 animals. At E16.5, 3 boxes of the same area were selected in control and mutant DG matrices. At P0, DG was delineated and separated into two areas: upper blade (UB) and lower blade (LB). At P7 and P14, DG was split into the DG three layers, based on DAPI staining. Analysis of the GFP+ cell distribution in IUE experiments was performed by counting GFP+ cells in three boxes within CA1 region and in the developing DG. Each CA1 boxes were subdivided into VZ, IZ and PCL compartments. The developing DG was subdivided into 1^{ry}, 2^{ry} and 3^{ry} matrix. The number of GFP+ cells for each compartment was expressed as a percentage of the total number of counted GFP+ cells for each region. Cell counts were performed on at least 3 consecutive rostral sections for each analysed brain using the counting tool of Adobe Photoshop CS6. A spreadsheet software and a two-tailed paired Student's t-test were used to analyse statistical significance between mutant and their controls (*p<0,05; **p<0,01; ***p<0,001). All graphs represent means ± s.e.m.

References:

Flore, G., Di Ruberto, G., Parisot, J., Sannino, S., Russo, F., Illingworth, E. A., Studer, M. and De Leonibus, E. (2016). Gradient COUP-TFI Expression Is Required for Functional Organization of the Hippocampal Septo-Temporal Longitudinal Axis. *Cereb Cortex*.

Pacary, E., Haas, M. A., Wildner, H., Azzarelli, R., Bell, D. M., Abrous, D. N. and Guillemot, F. (2012). Visualization and genetic manipulation of dendrites and spines in the mouse cerebral cortex and hippocampus using in utero electroporation. *Journal of visualized experiments : JoVE*.

Table S1. List of antibodies used in this study.

Antibody	Host species	Provider (reference)	Dilution
anti-cleaved Caspase3	rabbit	Cell Signaling (9661)	1:1000
anti-COUP-TFI	rabbit	Tripodi et al., 2004	1:1000
anti-COUP-TFI	mouse	Abcam (ab41858)	1:500
anti-GFAP	mouse	Sigma (G3893)	1:1000
anti-Ki67	rabbit	Abcam (ab833)	1:100
anti-Mcm2	rabbit	Abcam (ab4461)	1:1000
anti-NeuN	mouse	Millipore (MAB377)	1:100
anti-Prox1	rabbit	AngioBio (11-002)	1:1000
anti-Tbr1	rabbit	Abcam (ab31940)	1:1000
anti-Tbr2	chicken	Millipore (AB15894)	1:500
Alexa Fluor 488 anti-mouse/rabbit/chicken	goat	Fisher Scientific (10003482/10779623/10286672)	1:300
Alexa Fluor 555 anti-mouse/rabbit	goat	Fisher Scientific (10143952/10082602)	1:300
Alexa Fluor 647 anti-mouse/rabbit	goat	Fisher Scientific (10246452/10739574)	1:300
anti-rabbit IgG biotinylated	goat	Vector Laboratories (pk-6101)	1:300

Table S2. List of primers used in this study.

		FW	REV
for RT-PCR	COUP-TFI	TCCCATCGAAACTCTCATCC	AGTGGGCTGCTCTTGTTCC
	CXCR4	ATGGAACCGATCAGTGTGAGT	TGAAGTAGATGGTGGGCAGG
	B-Actin	ATGTGGATCAGCAAGCAGGA	GTGTAAAACGCAGCTCAGTAACA
for ChIP	CXCR4	ACAGTTCTACAGTCCTACACACAG	TCCTCTAGTTTTTGTGAGGTTTGAC